The structure-performance relationships in active center size-dependent Fenton-like catalysis: From nanoparticles to single atoms

Bingkun Huang [a,b], Zelin Wu [a,b], Hongyu Zhou [a,b], Xinhao Wang [a,b], Yang Liu [a,b], Heng Zhang [a,b], Zhaokun Xiong [a,b,*], Bo Lai [a,b,*]

[a] State Key Laboratory of Hydraulics and Mountain River Engineering, College of Architecture and Environment, Sichuan University, Chengdu 610065, China
[b] Sino-German Centre for Water and Health Research, Sichuan University, Chengdu 610065, China

ABSTRACT

Compared to nanocluster catalysts (NCCs) and nanoparticle catalysts (NPCs), single-atom catalysts (SACs) with isolated spatial sites and unique electronic structures generally demonstrate superior activity, selectivity, and stability. However, the correlation between the size of catalytic centers (ranging from nanoparticles to the atomic scale) and their performance in Fenton-like reactions remains unclear. In this review, we systematically outline the scale-regulated synthesis from NPCs to SACs, summarize the relationship of catalytic performance and mechanism to the active center scale, and emphasize the pivotal role played by the coordination microenvironment in dictating catalytic performance. Importantly, our analysis delves into the impact of the catalytic center scale on performance at the atomic level, specifically comparing isolated metal sites and metal-metal interactions, transcending the conventional consideration of active site density variation. To conclude, we highlight the challenges and future directions for research on structure-performance relationships, which are indispensable for the development of high-performance SAC architectures.

1. Introduction

With the increasing societal concerns for sustainable development and improved quality of life, the mitigation of water pollution has emerged as one of the pressing challenges [1,2]. Since its inception in 1987 [3], advanced oxidation processes (AOPs), which produce active species with high oxidation potential (e.g., $E^0(SO_4^{\bullet-}/SO_4^{2-}) = +2.60 \sim +3.10$ V$_{NHE}$ and $E^0(^{\bullet}OH/OH^- = +1.90 \sim +2.70$ V$_{NHE}$)), have been widely used to treat refractory and non-biodegradable organic pollutants that conventional water treatment cannot effectively remove [4–16]. The catalysts of AOPs are mainly divided into homogeneous catalysts and heterogeneous catalysts. Homogeneous catalysts, known for their highly dispersed and well-defined active sites, typically exhibit remarkable catalytic activity and selectivity. However, poor stability and recyclability limit the practical application of such catalysts [17, 18]. Heterogeneous catalysts address these concerns by offering enhanced stability and recyclability, but the low catalytic activity of large-sized metal particles loaded on conventional catalysts is a tremendous challenge [19,20].

The scale of the active center in heterogeneous catalysts is recognized as a critical parameter that significantly impacts their catalytic performance [21–23]. Given that reactions typically occur on the metal surface, metal atoms within nanoparticles (> 5 nm) are minimally involved in catalytic processes. In contrast, nanoclusters (~ 1 nm), particularly single atoms (~ 0.1 nm), can achieve nearly 100% atomic efficiency for a specified reaction (Fig. 1a) [22–25]. Consequently, compared with conventional nanoparticle catalysts (NPCs) or nanocluster catalysts (NCCs), single-atom catalysts (SACs) often exhibit exceptional catalytic activity. Since Zhang and co-workers first reported SACs in 2011 [26], SACs have led to an exponential increase in studies due to their unique geometric and electronic properties [27–35]. SACs establish a novel connection between homogeneous and heterogeneous catalysis, possessing well-defined structures and high activity akin to homogeneous catalysts, along with the stability and ease of separation typical of heterogeneous catalysts [36–38]. Novelty, while SACs typically result in high catalytic activity, a growing number of recent studies have found that NCCs or NPCs exert better catalytic activity due to interactions between single atoms and clusters or particles, which mark a

---

potentially transformative focus for future research in heterogeneous catalysts (Fig. 1b) [39–41].

The prevailing trend in current literature suggests that the catalytic activity increases as the scale of the metal active center decreases. However, in a departure from this commonality, an increasing number of studies have shown that, unlike conventional particulate catalysts with insufficient exposure of active sites, large metal-scale catalysts with well-defined active sites (diatomic catalysts, NCC, etc.) can exhibit superior catalytic performance compared to SACs [42–45]. The catalytic center scale affects not only the active site density but also the local chemical environment and electronic structure of the catalysts, such as coordination number, coordination composition, electron orbital, etc. [46–49]. Alterations in the coordination microenvironment and electronic structure will affect the adsorption and activation energy of the catalyst to the reactants (e.g., oxidants in Fenton-like reaction), which in turn affects the activity, selectivity and stability of the catalysts [49–52]. Considerable efforts have been devoted to developing synthetic strategies for SACs, and extending their applications in various catalytic reactions. To date, several valuable reviews on SACs in Fenton-like catalysis have been published, and the future opportunities and challenges of SACs in Fenton-like reactions have been put forward [53–57]. However, the current review mainly focuses on summarizing the advantages of SACs, the mechanisms involved in the effect of changes in the local chemical environment and electronic structure induced by changes in the catalytic site size on the catalytic performance have been overlooked. There is no systematic and rigorous review of the relationship between the structure and activity of catalytic sites in size-dependent Fenton-like catalysis. Therefore, systematically summarizing the structure-performance relationships between the active center and catalytic performance in Fenton-like reactions and its intrinsic mechanisms is of great significance.

In this comprehensive review, we delve into the remarkable progress made in synthesizing and applying active center size-dependent catalysts in Fenton-like catalysis and systematically summarize the structure-performance relationships at the atomic and electronic levels. Firstly, we review the synthesis of catalysts, which can regulate the scale of active metal sites from nanoparticles to single atoms. Subsequently, the structure-performance relationships of catalysts were analyzed from the aspects of activity, selectivity and stability. Additionally, we thoroughly conclude the intrinsic mechanisms that drive performance variations among catalysts with different metal scales. Finally, the main obstacles and future directions for the development of SACs are introduced from the perspective of active center-scale effects. This review will provide insightful and critical analysis for the design of advanced catalysts and contribute to a deeper understanding of structure-performance relationships in catalysis.

2. Synthesis modulation from NPCs to SACs

Precise regulation and design of the scale of different metal catalytic centers are decisive in revealing the deep connection between the structure and its catalytic performance. A formidable challenge persists in achieving synthetic regulation, spanning from NPCs to SACs. In recent years, a myriad of synthetic strategies for the preparation of SACs and NPCs have been reported. By finely adjusting the amount of introduced metal precursor, the synthesis temperature and the post-treatment steps, the degree of aggregation of metal atoms on the carrier can be effectively regulated, thus modulating the possibility of forming single atoms or nanoparticles. In addition, the strength of the interaction between the metal and the carrier material is one of the critical factors determining the scale of the metal active center. Strong interactions favor the stabilization of monodisperse metal atoms, while weaker interactions may result in the aggregation of metal atoms into nanoparticles. Based on recent advances, we will discuss several strategies for scale-regulated synthesis from NPCs to SACs. These strategies include the addition of metal precursors, etching techniques, temperature control, metal-
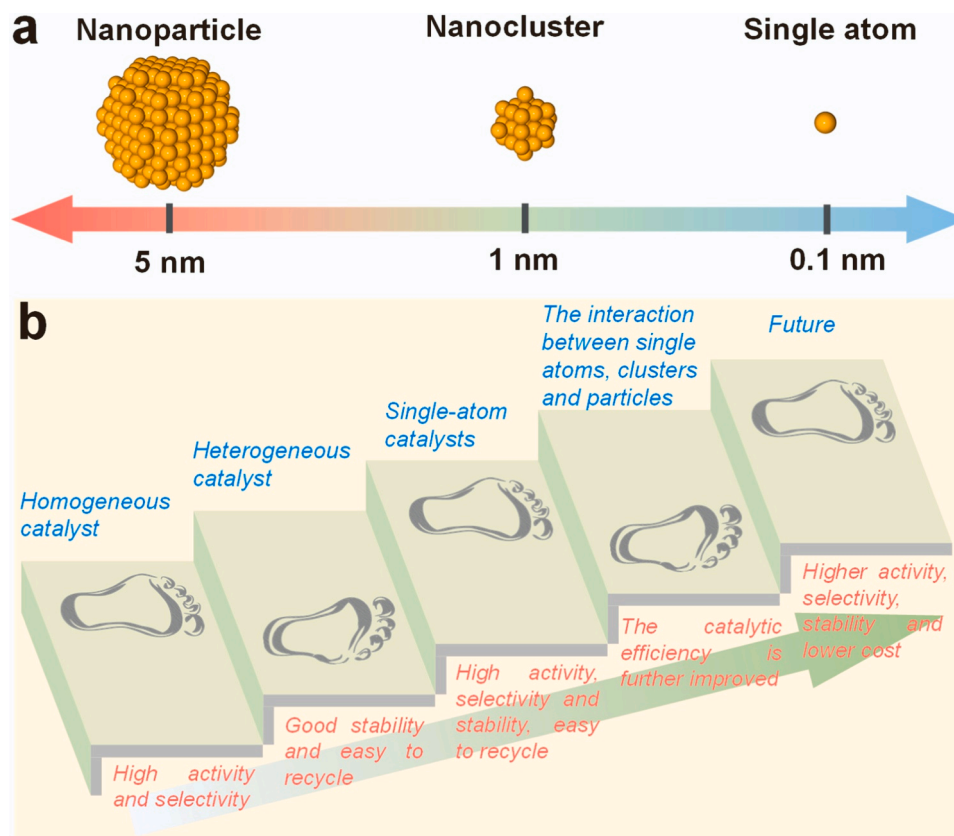

Fig. 1. (a) Typical geometry structure and size range of nanoparticle, nanocluster, and single-atom. (b) Development of catalysts in Fenton-like reactions.

support interactions, confined effects, and other advanced methods (Fig. 2).

2.1. Addition of metal precursors

The amount of metal precursor added greatly influences the metal morphology formed in the catalyst [58]. Individual metal atoms have higher surface energies and tend to aggregate to form large particles of metal species [25]. The carrier has certain fixing and limiting abilities for metal atoms. In broad terms, fewer metal precursors facilitate the dispersion of the metal under coordination or restriction, thereby promoting the formation of SACs. Conversely, an excess of metal precursors tends to induce aggregation, leading to the formation of nanoclusters or nanoparticles. Thus, the transition from NPCs to SACs can be effectively achieved by adjusting the amount of metal precursors added. Reducing the amount of metal precursors can not only reduce the cost, but also improve the catalytic performance of catalysts [53]. Han et al. achieved precise control over the Co form on the atomic scale by adjusting the ratio of Zn to Co in ZnCo-zeolitic imidazolate frameworks (ZIFs) [58]. When ZnCo = 8:1, Zn species sufficiently isolated Co species, resulting in the formation of Co-SACs. However, with an increased ratio of Zn to Co, Co species could not be thoroughly dispersed, leading to the formation of nanoclusters or nanoparticles (Fig. 3a). And catalysts with different active center scales prepared by applying this method are widely used in Fenton-like reactions [59–61]. Similarly, catalysts with different iron forms were successfully synthesized by adjusting the ratio of Fe $(NO_3)_3 \bullet 9\ H_2O$ to SBA-15 [62]. A proportion of 0.162 g Fe$(NO_3)_3 \bullet 9\ H_2O$ mixed with 0.672 g SBA-15 resulted in the formation of single Fe atom site-loaded SBA-15. However, when 0.162 g Fe$(NO_3)_3 \bullet 9\ H_2O$ was mixed with 0.4 g SBA-15, aggregated Fe site-loaded SBA-15 was formed. Reducing the proportion of metal precursors allows for relatively sufficient coordination sites in the support, facilitating the transformation from NPCs to SACs. In addition, the regulation of an appropriate atom distance is crucial for improving the activity and selectivity of the reaction. For example, the atomic distance was controlled by adjusting the amount of H_2PdCl_4 added in the synthesis process and successfully preparing the catalyst containing neighboring Pd single atoms instead of isolated Pd atoms [63]. They demonstrated that catalysts with adjacent Pd single atoms retained the high selectivity advantages of isolated Pd atoms, while the synergy between adjacent atoms greatly enhanced the catalytic activity.

2.2. Etching

The etching method is one of the most commonly employed techniques for achieving the conversion of NPCs to SACs. When the fixing and limiting ability of the carrier is insufficient, metal atoms will inevitably aggregate to form metal particles. Acid etching and related etching techniques can weaken intermetallic bonds and remove unstable metal atoms, thereby effectively eliminating metal nanoparticles formed by the aggregation of metal atoms and facilitating the transformation of nanoparticles into single atoms [64]. In general, acid reagents are the most widely used etchant. For example, in the quest for catalysts containing monodisperse Fe atoms, HCl was employed to etch away excess iron in Fe-NPCs, resulting in the successful obtaining of a catalyst with dispersed Fe sites [65]. In addition, Zhang et al. first dispersed Ni^{2+} on the defective graphene by the wet impregnation method and then pyrolyzed it, and Ni-NPC was generated. Subsequent leaching to remove excess Ni atoms led to the formation of Ni-SAC [66]. Most recently, as shown in Fig. 3b, a general and effective method was reported to obtain catalysts with atomic dispersion using ammonium iodide as an etching agent to remove excess metal aggregates at high temperatures [67]. In this strategy, excess metal nanoparticles formed volatile metal iodides by reacting with mild ammonium iodide at high temperatures, which could protect the atomic M-N_x moieties and the carbon substrate from considerable damage. While the etching method is commonly employed as a post-treatment for metal-based catalysts, enabling the transition from NPCs to SACs, it does not offer precise modulation of active sites. This limitation hinders its suitability for in-depth mechanistic investigations.

2.3. Temperature

It is well-established that isolated metal atoms possess high surface energy and are prone to aggregation [25,68]. Temperature affects the average kinetic energy of atoms or molecules and, thus the degree of their irregular thermal motion. Typically, high temperatures increase the degree of irregular thermal movement of metal atoms and thus accelerate the aggregation of isolated metal atoms [69]. The elevated temperature lowers the energy barrier, facilitating nucleation and promoting the formation of metal nanoparticles. Conversely, low temperatures increase the energy barrier and decrease the degree of irregular thermal movement, slowing down the nucleation rate and inhibiting the aggregation process [70]. Controlling the synthesis temperature presents a promising way to realize the transition from NPCs to SACs. Zhong et al. employed low temperatures to impede the diffusion rate of $PtCl_6^{2-}$ into carbon nanotubes, reducing the free energy of Pt atoms and minimizing the likelihood of aggregated Pt nanoparticles [71]. Besides, catalysts with different metal morphologies were successfully prepared by controlling the synthesis temperature [70]. At a synthesis temperature of 25 °C, Co nanoparticles nucleated and grew uninhibited. However, at a temperature of −60 °C, the nucleation of Co was suppressed, resulting in the formation of a Co-SAC with uniformly dispersed Co atoms (Fig. 3c). Similarly, using the effect of low temperature, Pt-SACs were also prepared [72,73]. The strategic use of temperature control emerges as a critical factor in achieving the desired morphological transition.

2.4. Metal-support interaction

The interaction strength of the metal-support is an essential factor affecting the metal morphology in the catalyst [74]. Successful restriction of the movement of metal atoms by the support is essential for preventing the formation of nanoparticles. Conversely, a strong metal-support interaction is conducive to achieving the complete dispersion of metal atoms, favoring the formation of single atoms. Designing defects and coordination groups on the carrier emerges as an effective strategy for capturing isolated metal atoms [75,76]. Li et al. demonstrated this approach by creating a large number of Ni^{2+} vacancy defects to stabilize monoatomic Pt species [77]. A high loading (2.3 wt %) Pt-SAC was successfully prepared using a simple wet impregnation method. Moreover, Zhang and co-workers reported the stabilization of dispersed Pt through a strong covalent metal-support interaction (CMSI)
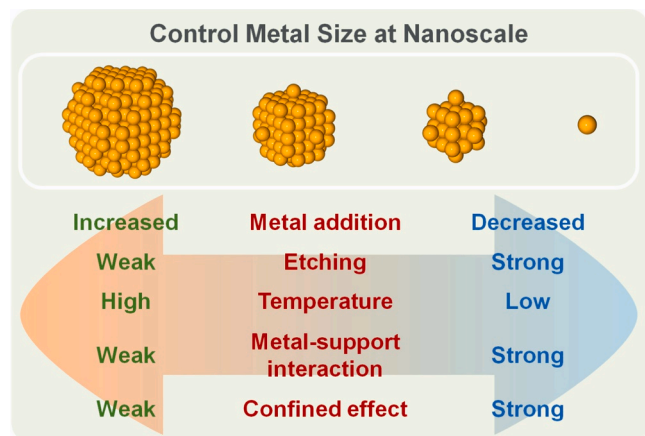

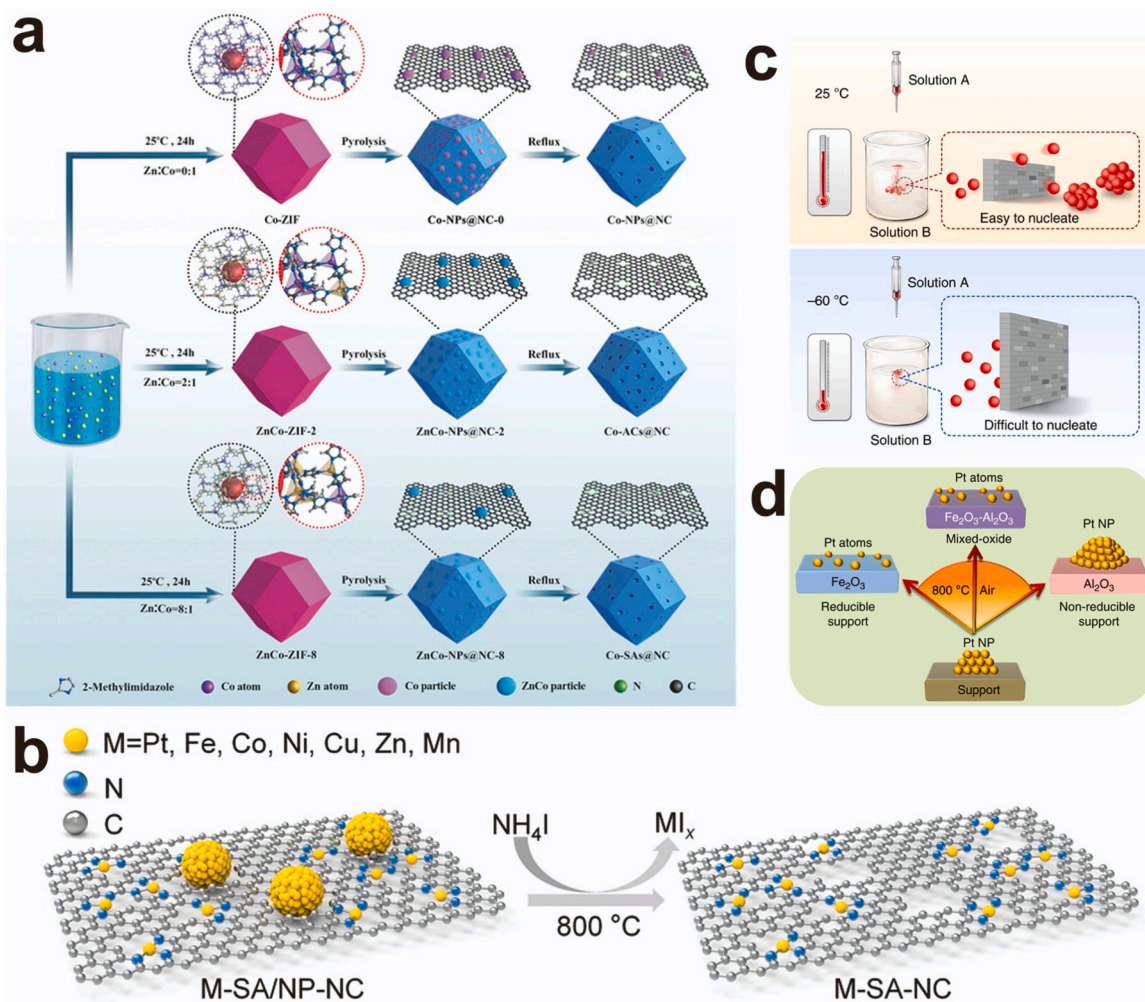**Fig. 2.** Summary of methods for modulating metal size at the nanoscale.

Fig. 3. (a) Preparation of the Co-NPs@NC, Co-ACs@NC, and CoSAs@NC catalysts. (b) The schematic diagram of the synthetic route toward M-SA-NC. (c) Schematic illustration of the ultra-low temperature solution reduction process. (d) Illustration of Pt nanoparticle sintering/dispersing on different supports.
(a) Reproduced with permission [58]. Copyright 2019, Wiley-VCH. (b) Reproduced with permission [67]. Copyright 2023, Wiley-VCH. (c) Reproduced with permission [70]. Copyright 2019, Springer Nature. (d) Reproduced with permission [74]. Copyright 2019, Springer Nature.

[74]. As shown in Fig. 3d, a strong CMSI was observed between Fe_2O_3 and Pt atoms, leading to the uniform dispersion of Pt atoms. In contrast, when the carrier was replaced with Al_2O_3, lacking CMSI with Pt atoms, Pt species aggregated. The stability tendency of isolated Pt atoms depends on the magnitude of the metal-support interaction, which can be adjusted by doping reducible Fe_2O_3 into non-reducible Al_2O_3. Choosing supports that provide ample anchoring sites and robust metal-support interactions is crucial to ensure high dispersion and stability of isolated metal atoms.

2.5. Confined effects

In addition to achieving the goal of capturing and restricting the movement of individual metal atoms through a strong metal-support interaction, the confinement effect offers an alternative mechanism. This effect involves restricting metal precursors to specific areas using different substances, thereby avoiding aggregation and facilitating the transformation from NPCs to SACs [17,78]. SACs can be easily prepared by confining a single metal precursor to a specific spatial structure. For example, in the synthesis of ZIF-8, ferric acetylacetonate ($Fe(acac)_3$) was introduced. [79]. The cavity dimensions of ZIF-8 (cavity diameter: 11.6 Å, pore diameter: 3.4 Å) ensured that only one $Fe(acac)_3$ molecule occupied a cavity, preventing its movement through the pore and promoting the synthesis of Fe-SACs. Similarly, ferrocene, with a molecular

diameter of 6.4 Å, could be confined within the cavity of ZIF-8, demonstrating the versatility of the confinement effect for the synthesis of Fe-SACs [80]. Besides, Fig. 4a showed that the introduction of Cu $(NO_3)_2$ precursors into template-occupied SBA-15 (TOS) through grinding resulted in the formation of monodisperse Cu species after calcination. In contrast, introducing $Cu(NO_3)_2$ into template-free SBA-15 (TFS) caused the aggregation of CuO [81]. In addition, the ball milling method also provides a simple means to achieve the spatial isolation of the metal precursor [82]. As displayed in Fig. 4b, Gan et al. ball-milled $Ce(Ac)_3$ and $Au(Ac)_3$ at a ratio of 1000:1 [83]. Because they have the same Ac ligand, $Au(Ac)_3$ could be thoroughly dispersed in Ce $(Ac)_3$, and a considerable enough spatial distance ensured that $Au(Ac)_3$ was difficult to aggregate during the pyrolysis process.

2.6. Other methods

The atomic layer deposition (ALD) method stands out as a straightforward approach to achieving the transformation from single atoms to nanoparticles. For instance, the size of Pt species could be easily adjusted by controlling the number of ALD cycles [84]. After 50, 100, and 150 cycles, the average particle size of Pt particles measures 0.5 nm, 1–2 nm, and 2–4 nm, respectively. Furthermore, although most reports mention that high temperatures quickly caused the aggregation of metal particles, Li et al. found that there were two reactions (sintering and
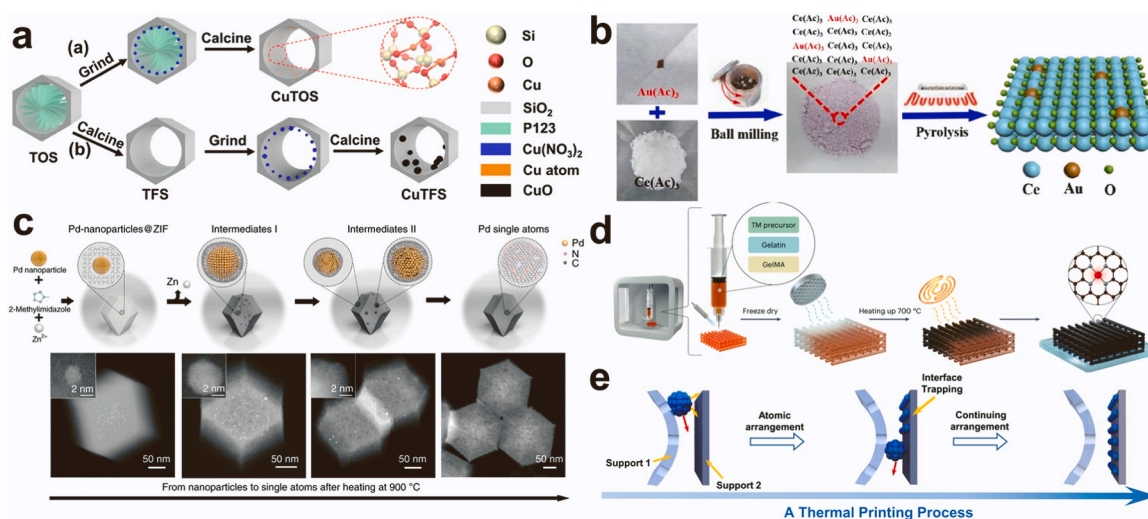
Fig. 4. (a) Schematic illustration for the formation of Cu single atoms. (b) Schematic illustration of the preparation process for Au$_1$/CeO$_2$. (c) HAADF-STEM images and high-resolution HAADF-STEM images (insets) of Pd-nanoparticles@ZIF-8, intermediate I, intermediate II and Pd single atoms. (d) Synthesis procedure for 3D-printed SACs. (e) Schematic illustration for thermal printing strategy.
(a) Reprinted with permission [81]. Copyright 2023, American Chemical Society. (b) Reproduced with permission [83]. Copyright 2020, Elsevier. (c) Reproduced with permission [85]. Copyright 2018, Springer Nature. (d) Reproduced with permission [89]. Copyright 2023, Springer Nature. (e) Reproduced with permission [90]. Copyright 2023, National Academy of Science.

atomization) in the pyrolysis process. The dominant reaction was different at different temperatures [85]. As depicted in Fig. 4c, Pt nanoparticles were first wrapped in ZIF-8. Sintering dominated at lower temperatures (300–900 °C), and Pt nanoparticles aggregated into larger nanoparticles. At higher temperatures (900–1000 °C), the atomization process took the initiative, and the large Pt nanoparticles began to disperse. Ultimately, Pt-SAC with fully dispersed Pt atoms was formed, showcasing the successful transformation from NPCs to SACs.

In recent advancements, three-dimensional (3D) printing technology has gained widespread application in the large-scale synthesis of substances with specific geometries [86]. Recognized for its simplicity, 3D printing directly fabricates target materials, avoiding complex wet chemical processes [87,88]. A recent study reported a straightforward and cost-effective 3D printing method for fabricating SACs [89]. As illustrated in Figs. 4d, 3D printing technology automatically constructs 3D structures from inks composed of a hydrogel containing gelatin and GelMA mixed with corresponding transition metal precursors. Subsequently, the pre-printed samples were undergone freeze-drying and pyrolysis processes to successfully synthesize SACs. Notably, this economical and straightforward method is suitable for the large-scale generation of different metal-based SACs, so it has the potential for a wide range of industrial applications. Moreover, Wu et al. described a thermal printing strategy that allows the fabrication of single-atom sites at the interface of different carriers, imparting high accessibility and excellent catalytic activity [90]. The strategy relies on the controlled migration of removable nanoparticles between two contacting substrates and the accompanying emission of atoms from the nanoparticle surface at high temperatures (Fig. 4e).

3. Structure-performance relationships from NPCs to SACs

Fenton-like catalysis is usually the process in which peroxides (e.g., peroxymonosulfate (PMS), peroxydisulfate (PDS) and hydrogen peroxide (H$_2$O$_2$)) are activated by a catalyst to produce active species with higher oxidative capacity [91,92]. The scale of the active center of the catalyst is one of the critical factors affecting the catalytic performance [59,61]. In this chapter, the relationship between the scale of metal centers and catalytic performance in non-homogeneous phase Fenton-like catalysis will be analyzed in terms of catalytic activity, catalytic selectivity and catalytic stability.

3.1. Catalytic activity

The scale of metal species plays a pivotal role in influencing the number of active sites and the coordination microenvironment, thereby significantly impacting catalytic performance [93–96]. As shown in Fig. 5a, SACs with smaller metal structures result in sufficient metal dispersion and maximum active site utilization, so SACs exhibit ultra-high catalytic activity in Fenton-like catalysis [97,98]. In general, compared to NPCs with aggregated metal sites, the SACs showed superior activity [96,99–101]. Noticeably, emerging studies suggest that catalysts containing larger-scale metal sites, such as dual-atom catalysts or NCCs, may display higher catalytic activity than SACs due to the optimization of the electronic structure of the active site caused by metal-metal interactions (Fig. 5b) [44,102–104].

In a recent comprehensive study, Wu et al. systematically compared the catalytic performance of SACs, NCCs, and NPCs [59]. After normalization, they found that SACs exhibited the highest mass activity (Fig. 6a). Likewise, Gao et al. normalized the apparent rate constant according to the weight of cobalt in the catalyst, revealing that Co-SACs with well-dispersed active sites exhibited approximately a 6-fold higher quality activity than Co-NPCs (Fig. 6b) [91]. Moreover, investigators analyzed the relationship between metal content and reaction rate [105]. The catalytic performance of Fe-SACs improved with the increase in the amount of added iron precursors, showing a well-matched reaction rate constant with active site density (R^2 = 0.976) (Fig. 6c). And a similar phenomenon was observed in the study of Li and co-workers [106]. However, some studies reported that catalytic performance initially increased and then decreased with the growing amount of added metal precursor (Fig. 6d) [99]. This is because the catalytic activity increased as the active site density increased, but the excess metal atoms tend to aggregate into large-sized metal particles due to the larger metal surface energy.

Contrary to the notion that smaller metal size always translates to superior catalytic activity, some studies have intriguingly discovered that nanoclusters may exhibit surprising performance [40,41,107–110]. For example, in the coexistence system of ultra-small clusters and single-atom Fe sites, the removal efficiency of methylene blue (MB) was found to be higher than that of the pure Fe single-atom system [40]. The catalytic performance, when normalized by the weight of iron in each catalyst, increased as the cluster/single-atom ratio increased, indicating
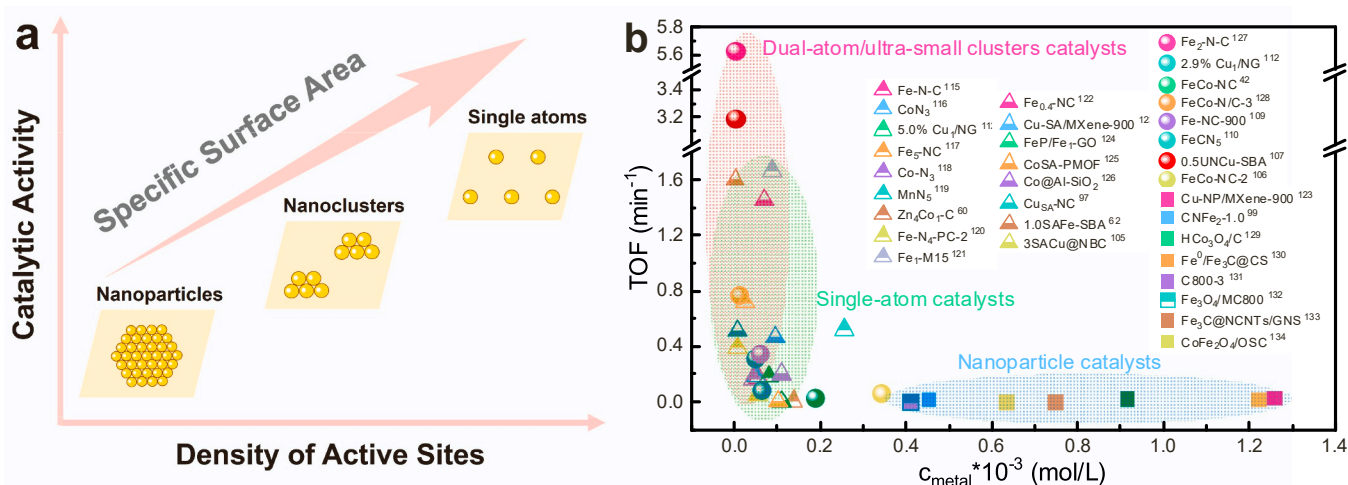
Fig. 5. (a) The relationship between the density of active sites and catalytic activity. (b) Relationship between the moles concentration of metal species of various metal-based catalysts and their catalytic performances in Fenton-like catalysis.
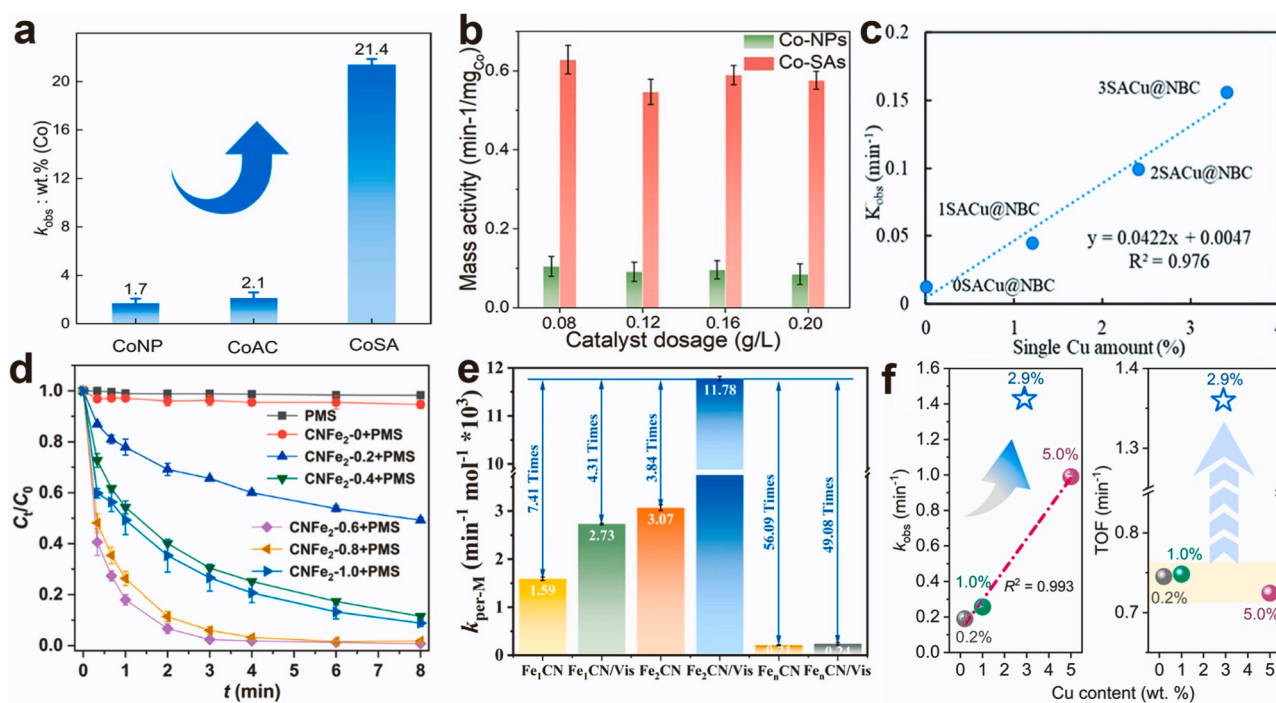

Fig. 6. (a) Normalized catalytic activity (k-value) of different samples. (b) The reaction rate constants normalized by the weight of Co in different systems. (c) The rate constants of BPA degradation in different activator/PMS systems. (d) Degradation kinetic curves of SMX by PMS and CNFe$_2$-x (x = 0–1.0) via PMS activation. (e) Normalized k_{obs} by per mole site of different systems. (f) First-order rate constants and TOFs of BPA removal by Cu$_1$/NG with different Cu site densities activating PDS.
(a) Reprinted with permission [59]. Copyright 2023, American Chemical Society. (b) Reproduced with permission [91]. Copyright 2020, Wiley-VCH. (c) Reproduced with permission [105]. Copyright 2021, The Royal Society of Chemistry. (d) Reproduced with permission [99]. Copyright 2022, Elsevier. (e) Reprinted with permission [111]. Copyright 2022, American Chemical Society. (f) Reproduced with permission [112]. Copyright 2022, Wiley-VCH.

that the catalytic activity of clusters surpassed that of single atoms. In another study, Li et al. normalized the pseudo-first-order reaction rate constant (k_{obs}) according to the iron content in the catalyst. The Fe$_2$CN/Vis/PMS system exhibited high catalytic activity attributed to the higher intrinsic activity of the Fe$_2$N$_6$ coordination configuration compared to the Fe$_1$N$_4$ coordination configuration, rather than simply an increase in the number of active sites (Fig. 6e) [111]. Furthermore, a suitable Cu-Cu distance was found to be beneficial in improving the intrinsic activity of PDS activation [112]. As shown in Fig. 6f, k_{obs} exhibited a high positive correlation (R^2 = 0.993) for Cu content in the

range of 0.2%, 1.0% and 5.0% Cu$_1$/NG. However, 2.9% Cu$_1$/NG corresponding to Cu-Cu sites with a distance of 5.3 Å broke this trend, and its kinetic performance and turnover frequency (TOF) were better than the other samples. Besides, ultrafine CuO nanoclusters and Cu single atoms were immobilized on a typical mesoporous silica SBA-15 (UNCuSBA) for a Fenton-like reaction [107]. After normalizing the Cu mass, the reaction rate constant of UNCuSBA was 18 times that of APCu-SBA containing aggregated CuO particles. Besides, Bi et al. found that Ru-NPCs activate PMS more efficiently than Ru-SACs due to enhanced adsorption of Ru-NPCs to PMS and that Ru-NPCs can lower the

energy barrier by providing dimerization of *O intermediates into adsorbed $^1O_2$ [113]. Moreover, through the self-assembly of Cu_5 nanoclusters on the surface of FeS_2 (001), Ling and colleagues constructed Cu-Fe catalytic sites for selective activation of H_2O_2 and efficient removal of pollutants [114]. These studies collectively demonstrate that nanoclusters may exhibit remarkable catalytic performance, even better than single atoms. So, in addition to the geometric configuration of the active center, the electronic configuration of the active center should also be considered to influence the catalytic performance.

The catalytic performance comparison of recently reported SACs, NCCs and NPCs in Fenton-like catalysis is shown in Table 1, in which the green, red and blue backgrounds represent SACs, dual-atom or ultra-small cluster catalysts and NPCs, respectively. Notably, it is widely acknowledged that SACs, with their increased active site exposure, often exhibit higher activity. Intriguingly, a recent trend in the literature suggests that dual atoms or clusters may demonstrate performance advantages over single atoms, potentially owing to their unique coordination and electronic structures. We will explore this phenomenon in greater detail in Chapter 4, analyzing the distinctive features of dual atoms and clusters that contribute to their catalytic performance. This discussion aims to provide insights into the relationship between the effectiveness and different catalytic architectures in Fenton-like reactions.

3.2. Catalytic selectivity

Compared with NPCs, the active sites in SACs are well dispersed. Theoretically, when the active site is sufficiently homogeneous, the active species produced by each active site should also be uniform. Therefore, SACs not only showcase high catalytic activity but also achieve ultra-high selectivity, as supported by a body of literature [135–138]. The explicit definition of active sites in SACs, coupled with the clarity of the active species, enhances the understanding of the catalytic mechanism. In addition, in Fenton-like catalysis, metal particles typically have stronger adsorption energy for oxidants, which causes the O-O bond to be elongated and thus more easily broken to generate radicals. Whereas single metal atoms have weaker adsorption energy to the oxidants, most of the active species in SAC systems are dominated by non-radicals due to the difficulty of breaking the O-O bond (Fig. 7) [59,61].

In the study conducted by Sheng and colleagues, the selectivity of iron species at different scales (single atoms and oxide clusters) for catalyzing H_2O_2 in photo-Fenton was rigorously evaluated [136]. In-situ Fourier transform infrared (FT-IR) studies (Fig. 8a-b) and density functional theory (DFT) calculations (Fig. 8c-d) showed that the Fe-SAC underwent more pronounced surface hydroxylation than the oxide cluster catalyst during H_2O_2 activation, and the adsorption energy of surface hydroxyl groups on Fe-SAC was significantly higher. The change

Table 1
The catalytic performance comparison of recently reported SACs, NCCs and NPCs in Fenton-like catalysis.

Catalyst (g L^{-1})	Metal (wt%)	Pollutants (mM)	Removal efficiency	Reaction time (min)	TOF[a] (min^{-1})	Oxidant	Ref.
Fe-N-C (0.1)	Fe (3.1)	Bisphenol A (BPA, 0.1)	100%	10	0.180	PMS	[115]
CoN_3 (0.1)	Co (2.9)	Rhodamine B (RhB, 0.045)	100%	5	0.183	PMS	[116]
5.0% Cu_1/NG (0.1)	Cu (5.0)	BPA (0.088)	100%	6	0.186	PDS	[112]
Fe_5-NC (0.2)	Fe (0.65)	Oxalic acid (OA, 1.111)	≈90%	60	0.716	O_3	[117]
Co-N_3 (0.1)	Co (2.45)	Carbamazepine (CBZ, 0.042)	100%	6	0.168	PMS	[118]
MnN_5 (0.5)	Mn (2.8)	p-chlorophenol (4-CP, 0.078)	100%	6	0.051	PMS	[119]
Zn_4Co_1-C (0.1)	Co (8.06)	Phenol (0.213)	100%	3	0.519	PMS	[60]
Fe-N_4-PC-2 (0.03)	Fe (1.23)	Sulfamethoxazole (SMX, 0.038)	100%	15	0.393	PMS	[120]
Fe_1-M15 (0.1)	Fe (4.8)	BPA (0.096)	100%	0.67	1.667	PMS	[121]
$Fe_{0.4}$-NC (0.16)	Fe (2.4)	BPA (0.1)	100%	1	1.454	PMS	[122]
Cu-SA/MXene-900 (0.5)	Cu (1.19)	BPA (0.438)	100%	10	0.468	PMS	[123]
FeP/Fe_1-GO (0.15)	Fe (4.1)	Tetracycline (0.023)	100%	30	0.007	Photo-H_2O_2	[124]
CoSA-PMOF (0.1)	Co (6.1)	Moxifloxacin (0.001)	≈100%	6	0.002	PMS	[125]
Co@Al-SiO_2 (0.1)	Co (6.5)	Chlorobenzene (0.178)	100%	8	0.202	PMS	[126]
Cu_{SA}-NC (0.04)	Cu (1.03)	2,4-Dichlorophenol (0.1)	100%	30	0.514	PDS	[97]
1.0SAFe-SBA (0.1)	Fe (0.056)	p-hydroxybenzoic acid (HBA, 0.145)	100%	90	1.607	H_2O_2	[62]
3SACu@NBC (0.1)	Cu (3.41)	BPA (0.088)	100%	30	0.055	PMS	[105]
Fe_2-N-C (0.01)	Fe (0.51)	RhB (0.021)	≈98%	4	5.634	PMS	[127]
2.9% Cu_1/NG (0.1)	Cu (2.9)	BPA (0.008)	100%	6	0.321	PDS	[112]
FeCo-NC (0.2)	Fe (2.01) Co (3.32)	Phenol (0.213)	100%	30	0.038	PMS	[42]
FeCo-N/C-3 (0.05)	Fe (0.74) Co (0.46)	Phenol (0.163)	100%	20	0.774	PMS	[128]
Fe-NC-900 (0.8)	Fe (0.41)	RhB (0.209)	99.5%	10	0.354	PMS	[109]
$FeCN_5$ (0.5)	Fe (0.68)	Methylene blue (MB, 0.053)	≈100%	10	0.087	H_2O_2	[110]
0.5UNCu-SBA (0.2)	Cu (0.032)	HBA (0.145)	100%	45	3.199	H_2O_2	[107]
FeCo-NC-2 (0.1)	Fe (6.3) Co (13.5)	BPA (0.088)	100%	4	0.064	PMS	[106]
Cu-NP/MXene-900 (0.5)	Cu (15.99)	BPA (0.438)	89.89%	10	0.031	PMS	[123]
$CNFe_2$-1.0 (0.08)	Fe (31.56)	SMX (0.079)	≈90%	8	0.020	PMS	[99]
HCo_3O_4/C (0.1)	Co (53.89)	BPA (0.088)	100%	4	0.024	PMS	[129]
Fe^0/Fe_3C@CS (0.2)	Fe (34.12)	Phenol (0.213)	100%	10	0.017	PMS	[130]
C800–3 (0.1)	Fe (22.95)	BPA (0.088)	100%	90	0.002	PMS	[131]
Fe_3O_4/MC800 (0.2)	Fe (11.44)	HBA (0.072)	100%	30	0.006	PMS	[132]
Fe_3C@NCNTs/GNS (0.2)	Fe (20.9)	BPA (0.088)	97.8%	30	0.004	PMS	[133]
$CoFe_2O_4$/OSC (0.5)	Fe (15.23) Co (2.59)	Norfloxacin (0.03)	90%	60	0.0004	PMS	[134]

$$^aTOF = \frac{\text{moles of reactant converted}}{\text{moles of active sites} \times \text{reaction time}} = \frac{\Delta n(\text{reactant})}{n_{metal} \times t} = \frac{\Delta n(\text{reactant}) \times M_{metal}}{m_{metal} \times \omega_{metal} \times t} = \frac{\Delta c(\text{reactant}) \times M_{metal}}{M(\text{recatant}) \times c_{metal} \times \omega_{metal} \times t}$$

where Δn(reactant) is the moles of reactant converted, n_{metal} is the moles of metal species, M_{metal} is the atomic weight of metal species, m_{metal} is the mass dosing of catalysts, ω_{metal} is the mass concentration of metal species in the catalysts, Δc(reactant) is the mole concentration of reactant converted, $M_{reactant}$ is the atomic weight of reactant, c_{metal} is the mole concentration of metal species, and t is the reaction time.
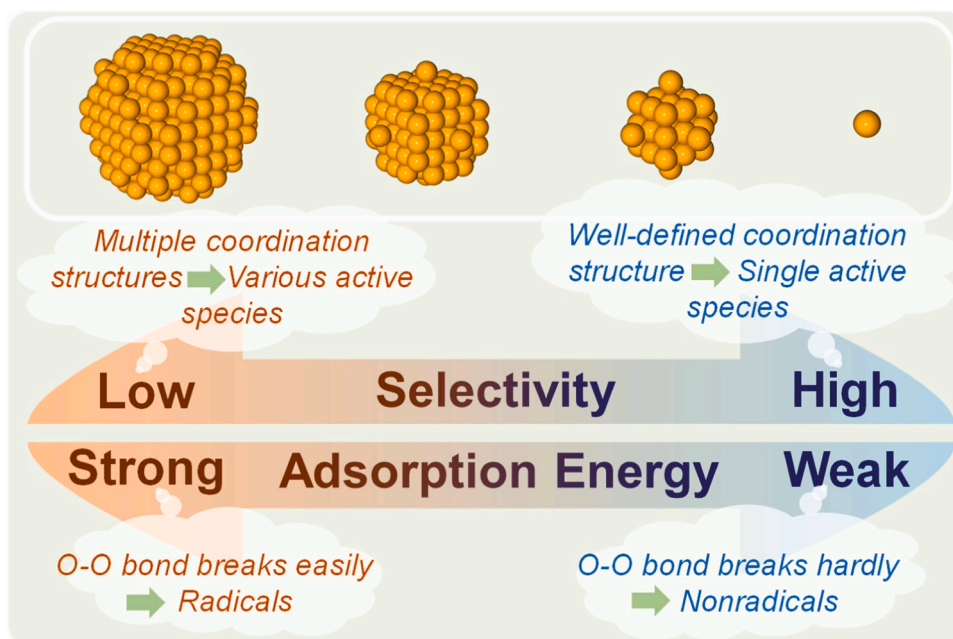
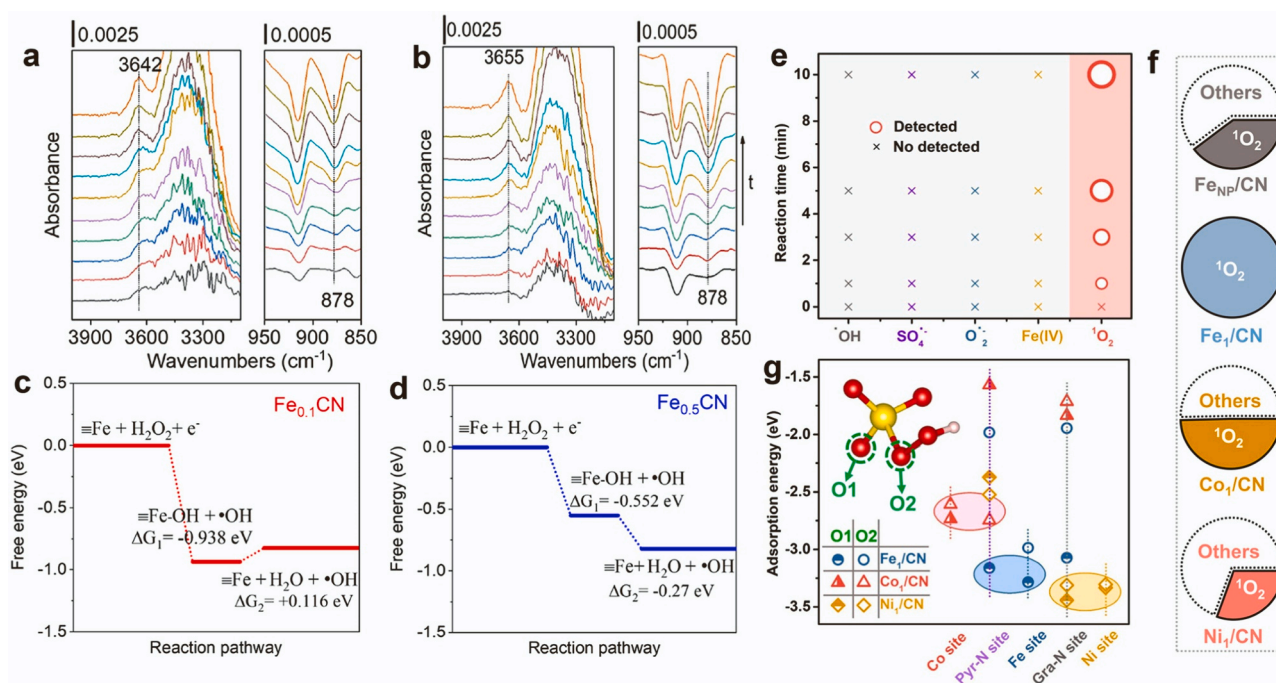**Fig. 7.** Schematic of catalytic selectivity with active center size-dependent Fenton-like catalysis.

Fig. 8. Series of IR spectra collected after different times illumination on (a) $Fe_{0.1}CN/H_2O_2$ and (b) $Fe_{0.5}CN/H_2O_2$. Gibbs free energy diagrams of one-electron H_2O_2 reduction on (c) $Fe_{0.1}CN$ and (d) $Fe_{0.5}CN$. (e) Qualitative and quantitative analyses of active species present in Fe_1/CN activated PMS system. (f) The proportion of $^1O_2$ in different catalysts activated PMS systems. (g) The adsorption energies of PMS onto the different sites of catalysts (inset: molecular model of PMS). (a-d) Reprinted with permission [136]. Copyright 2022, American Chemical Society. (e-g) Reproduced with permission [137]. Copyright 2021, Wiley-VCH.

in the adsorption mode of H_2O_2 in the single-atom system is more favorable for the selective oxidative conversion of H_2O_2 to $O_2^{\bullet-}/^1O_2$, while H_2O_2 is more inclined to be converted to $^{\bullet}OH$ in the catalysts with abundant oxide clusters. In addition, as displayed in Fig. 8e-f, it was revealed that when Fe species was present in the form of nanoparticles, PMS was activated to generate various reactive oxygen species (ROS), including singlet oxygen ($^1O_2$), $SO_4^{\bullet-}$, $^{\bullet}OH$ and $O_2^{\bullet-}$. In contrast, when the size of Fe was reduced to single-atom, the proportion of $^1O_2$ produced increased from 43% to 100% [137]. Although the proportion of $^1O_2$

generated in the Co-based and Ni-based catalyst systems was not 100%, DFT calculations proved that this was because the generation of ROS was also affected by the metal species and the different O adsorption sites of PMS (Fig. 8g). Moreover, atomically dispersed cobalt on nitrogen-co-doped carbon (Co-SA) was used to precisely regulate the $^1O_2$ generation during PMS activation at the atomic scale [135]. The experiments and DFT calculations showed that CoN_{2+2} was the active site, and the yield of singlet oxygen was as high as 98.89%. Similarly, Zhao et al. also verified the existence of CoN_{2+2} and achieved 100%

conversion of PMS to $^1O_2$ [139].

ROS generated during peroxide activation can be divided into radicals ($SO_4^{\bullet-}$ and $^{\bullet}OH$, etc.) and non-radicals ($^1O_2$ and high-valent metal-oxo species, etc.). Non-radical oxidation has weak oxidation capacity, which makes it challenging to achieve high mineralization rate of wastewater. Radical oxidation is highly oxidizing and can attack pollutants indiscriminately, but it also suffers from a short lifetime and low ROS utilization. Therefore, in order to meet the treatment requirements of different wastewater, it is of great environmental significance to research the adjustable conversion of radical and non-radical reaction pathways [140]. Recently, our group employed DFT to illustrate that the dominant adsorption energies of Co-SAC, Co-NCC, and Co-NPC on PMS are −6.475 eV, −8.170 eV, and −11.700 eV, respectively, corresponding to O-O bond lengths of 1.461 Å, 1.496 Å, and 1.747 Å [59]. Notably, the O-O bond distance was found to influence the likelihood of breaking, with longer distances favoring the production of $SO_4^{\bullet-}$ and $^{\bullet}OH$. The combined analysis of Gibbs free energy revealed that Co-NPC exhibited a higher likelihood of producing $SO_4^{\bullet-}$ and $^{\bullet}OH$ (Fig. 9a), whereas Co-SAC demonstrated a stronger inclination towards generating $^1O_2$ (Fig. 9b-d). In addition, the modulation of the reaction mechanism and pollutant degradation pathway can be achieved by tuning the scale of active center [61]. The evolution from $SO_4^{\bullet-}$ and $^{\bullet}OH$ to $^1O_2$ was achieved through the modulation of the scale of Co species from nanoparticles to single atoms (Fig. 9e). Different sites of organic molecules are attacked differently by radicals and non-radicals (Fig. 9f), which can be indicated by the calculated Fukui index [141,142]. Moreover, the d-band center and adsorption energy were modulated through the synergistic

interaction between homo-diatomic Fe sites, and the optimization of the electronic structure achieved efficient and selective activation of PMS (Fig. 9g) [111]. Furthermore, it has also been found that high-valent metal-oxo species emerged with higher selectivity in recent studies of SACs-based Fenton-like catalysis [119,122,143,144]. The selective generation of ROS in SACs has made outstanding contributions to exploring mechanisms and designing target catalysts.

The selective production of ROS leads to selective degradation, a crucial aspect in the realm of catalytic processes for wastewater treatment. The mild oxidizing capability of non-radicals can effectively avoid the competitive reaction of ROS and organic/inorganic co-existing substrates, thereby realizing the selective removal of the target contaminant [145,146]. Ultra-high $^1O_2$ generation selectivity was achieved by regulating Co species scale and coordination [60]. The selective removal rate of phenol in the mixed solution of phenol/benzoic acid was up to 98% by using the property of non-radical selective oxidation (Fig. 9h). In addition, the properties of pollutants themselves also affect the degradation mechanism. Yang et al. demonstrated that radical oxidation and non-radical electron-transfer pathways exist simultaneously in the Co-N$_4$-C/PMS system [147]. Pollutants with high redox potential were mainly degraded by radicals, while the oxidation of low-redox pollutants is mainly dominated by the electron-transfer mechanism (Fig. 9i). Moreover, substrate-dependent behavior was also found by Ren and co-workers [117]. They used single-atom Fe-N$_4$ sites to selectively induce non-radical pathways (surface-adsorbed atomic oxygen ($^*O_{ad}$) and $^1O_2$) for catalytic ozonation. The adsorption of oxalic acid on the catalyst surface predominantly led to degradation by $^*O_{ad}$,
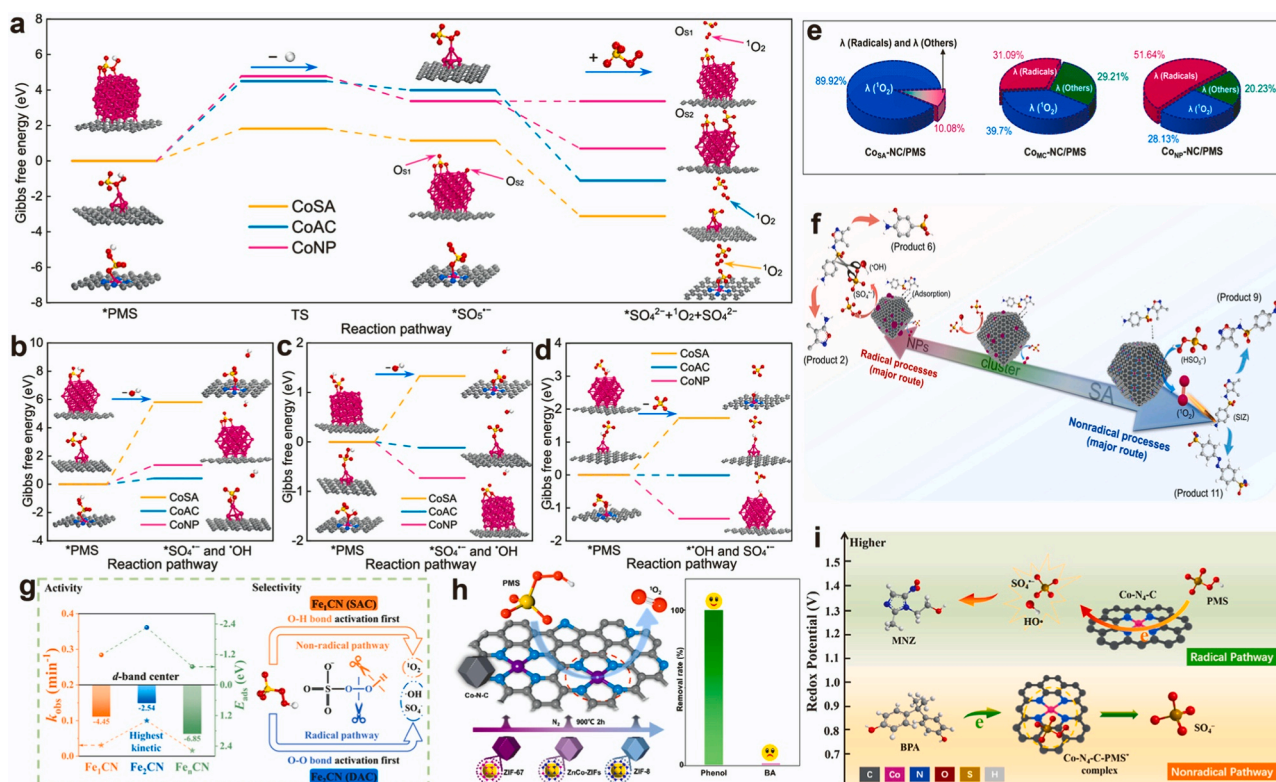

Fig. 9. (a) Reaction pathways of the dominant PMS adsorption model at Co-SAC, Co-NCC, and Co-NPC for $^1O_2$ generation. Reaction pathways of the (b) dominant and (c) inferior PMS adsorption models at Co-SAC, Co-NCC, and Co-NPC for $^{\bullet}OH$ generation. (d) Reaction pathways of the PMS hydroxyl oxygen adsorption model at Co-SAC, Co-NCC, and Co-NPC for $SO_4^{\bullet-}$ generation. (e) The proportion of $^1O_2$, $^{\bullet}OH$ and $SO_4^{\bullet-}$ in different catalytic systems. (f) Catalytic mechanisms of active center size-dependent catalysts for PMS activation. (g) Correlation of different iron coordination models with activity and selectivity. (h) The evolution of ROS and selective oxidation of micropollutants in complex wastewater via regulating the molecular structure of catalysts. (i) Pollutant-dependent radical and nonradical pathways for selective degradation in the Co-N$_4$-C/PMS system. (a-d) Reprinted with permission [59]. Copyright 2023, American Chemical Society. (e-f) Reproduced with permission [61]. Copyright 2023, Elsevier. (g) Reprinted with permission [111]. Copyright 2022, American Chemical Society. (h) Reprinted with permission [60]. Copyright 2022, American Chemical Society. (i) Reprinted with permission [147]. Copyright 2022, American Chemical Society.

while O_3 and $^1O_2$ played a more significant role in removing p-hydroxybenzoic in the bulk solution. In conclusion, non-radical oxidation excels in the selective removal of pollutants, while radical oxidation proves more suitable for rapidly addressing chemical oxygen demand (COD) and other organic matter in wastewater. Hence, it is of great environmental significance to rationally regulate the scale of active centers to achieve the selective generation of ROS, meeting the different treatment requirements of wastewater.

3.3. Catalytic stability

The stability and reusability of a catalyst are paramount considerations for its practical application [100,148–150]. During the synthesis of SACs, carriers rich in coordination elements such as nitrogen (N) or sulfur (S) are commonly chosen to prevent metal aggregation. These elements act as a kind of "claw", effectively binding metal ions and contributing to the formation of a stable coordination structure [53, 151]. Therefore, catalysts with smaller-scale metal centers actually possess relatively high stable coordination structure, and more and more studies have demonstrated the ultra-high stability (low metal leaching and slow weakening of activity) of SACs in Fenton-like catalysis (Fig. 10) [9,125,152,153].

To assess stability under operational conditions, researchers have expanded beyond traditional cycling experiments to incorporate continuous flow experiments, providing a more realistic simulation of practical applications [152,154–156]. These experiments are typically conducted using either columnar or membranous Fenton reactors (Fig. 11). Column reactors, with their longer hydraulic retention time, offer increased applicability. On the other hand, membrane reactors leverage a large contact surface and low flow resistance due to membrane properties, although this design presents challenges to the mechanical strength of the membrane reactors.

In 2020, Cui et al. designed the SACs Fenton filter (Fig. 12a) [152]. Remarkably, after 200 hours of operation, equivalent to filtering 2 liters of wastewater, the dye removal rate remained consistently at 100% (Fig. 12b). This device-level demonstration represented a significant step forward in validating the practical application potential of SACs. Our previous work investigated metal leaching in Co-NPC, Co-NCC, and Co-SAC systems (Fig. 12c). Notably, Co^{2+} leaching in Co-SAC was significantly lower compared to Co-NPC and Co-NCC. By comparing

Co-SAC, Co-NCC and Co-NPC, the pollutant degradation efficiency was found to decrease by 2%, 24% and 38% after five cycles, respectively (Fig. 12d). The high metal ion leaching and the rapid decrease in catalytic efficiency illustrate that NPCs are less stable than NCCs than SACs, a trend consistently observed in continuous flow experiments for pollutant removal (Fig. 12e). Similarly, Fe-SAC demonstrated almost 100% acyclovir removal efficiency in continuous flow experiments at 160 h of continuous treatment (Fig. 12f-g) [151]. Moreover, the fabricated Co-SAC was used in a continuous flow reactor and achieved almost 100% BPA removal efficiency during continuous operation for 168 h with a low Co ion leaching rate, indicating that Co-SAC has good catalytic activity and durability [157]. In addition, they further verified the excellent stability of Co-SAC by comparing the X-ray diffraction (XRD) pattern and high-angle annular dark-field scanning transmission electron microscopy (HAADF-STEM) images of Co-SAC after catalytic reaction with the fresh catalyst.

Compared with column reactors, membrane reactors have more significant challenges due to their higher water flux and shorter hydraulic residence time (Fig. 11) [158–160]. Typically, hydraulic retention times in membranous Fenton reactors are less than 1 second. Ma and colleagues designed catalytic membranes supported with Cu-SAC (Cu_1-M) and Cu_{nano} (Cu_{nano}-M) [160]. Cu_1-M exhibited stable acetaminophen removal for 300 min of continuous filtration with only a slight decrease in the catalytic activity. Conversely, the water purification performance of Cu_{nano}-M dropped dramatically over time, with the membrane completely inactive after 300 min (Fig. 12h). The stability of Cu_1-M is attributed to the electron-rich reaction carrier (S group), which maintained the low oxidation state of Cu atoms for catalysis. However, there are not enough electrons available for Cu reduction in Cu_{nano}-M (Fig. 12i). In addition, $Co-N_3O_1$ was used in the designed membrane reactor, and it was found that the residence time of water flow in PVDF/Co was only 312 ms [153]. The degradation efficiency of CIP in PVDF/Co/PMS system remained 97.5% within 10 h, and total organic carbon (TOC) removal efficiency was over 50%, indicating the high practical application potential of the PVDF/Co/PMS system. Furthermore, the low Co^{2+} leaching demonstrated the stable coordination between Co atoms and C_3N_4. Recently, ceramic membrane (CM) has been used as an excellent catalytic membrane carrier for Fenton-like continuous oxidation reaction because of its oxidation resistance, high mechanical strength and good chemical stability (Fig. 12j) [161].
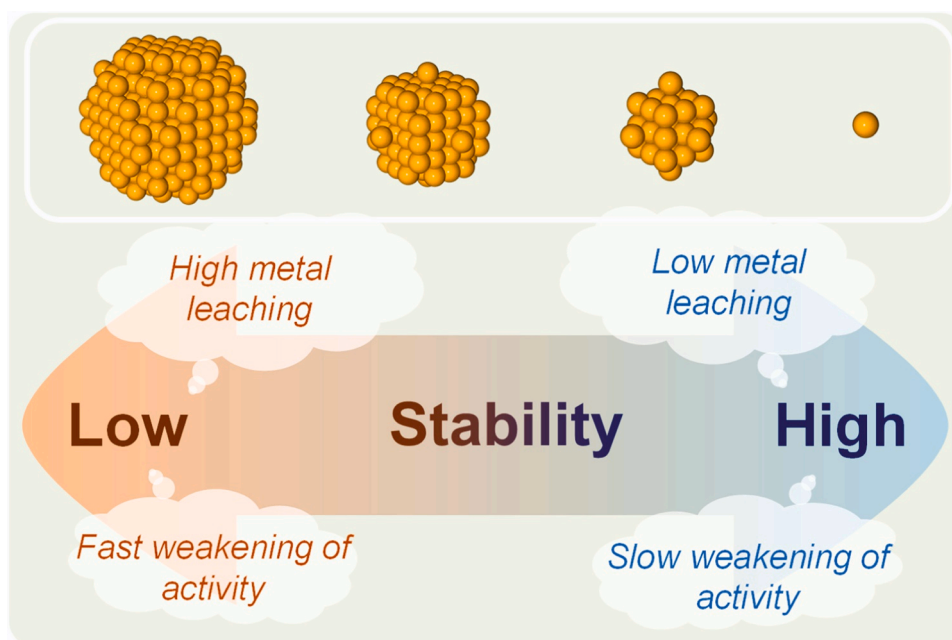

Fig. 10. Schematic of catalytic stability with size-dependent metal center in Fenton-like catalysis.
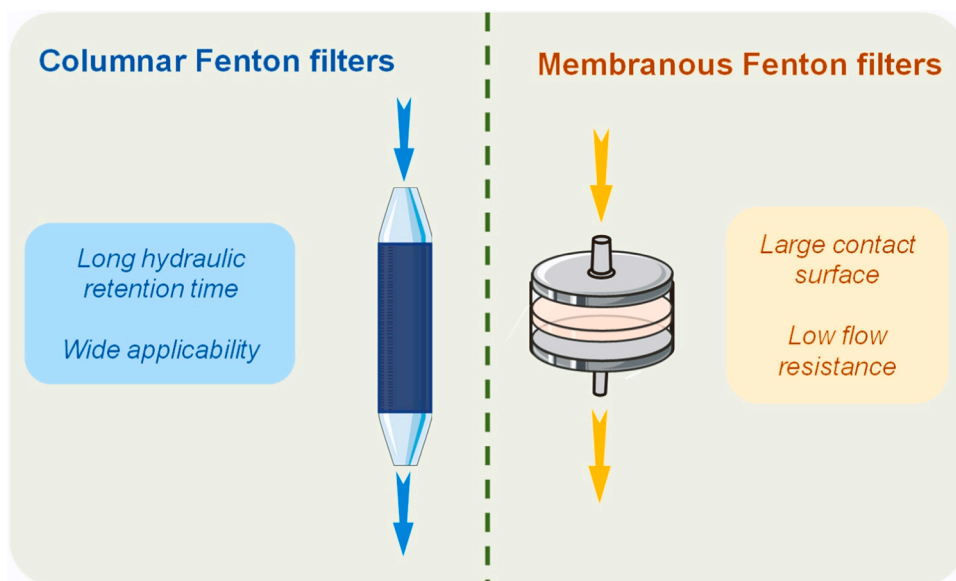
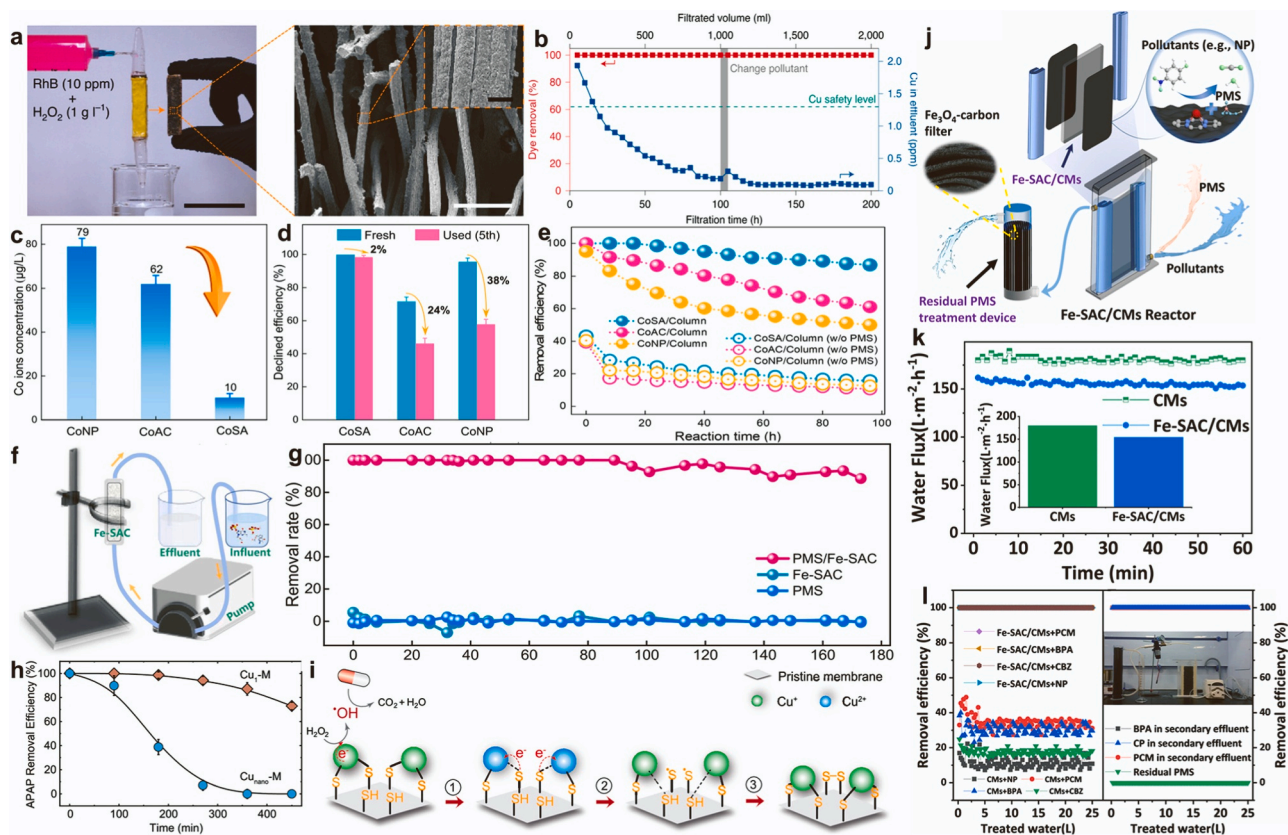**Fig. 11.** Schematic of columnar and membranous Fenton filters.

Fig. 12. (a) Image of a proof-of-concept Fenton filter and SEM image of the filter medium. (b) Dye removal and Cu concentration in the effluent as functions of filtration time. (c) Co^{2+} leaching in different catalytic systems. (d) Decline of 16 min degradation rate for Co-SAC, Co-NCC, and Co-NPC after five cycles. (e) Simulated sulfisoxazol treatment by the continuous-flow reactor. (f) Diagram of circulating flow experimental apparatus. (g) Water purification effects in fixed bed reactor. (h) Acetaminophen removal efficiency by the catalytic membranes during filtration. (i) Proposed mechanism for the highly efficient and durable Cu1-M-driven water purification. (j) Scheme of Fe-SAC/CMs for continuous water purification. (k) Water flux of bare CMs and Fe-SAC/CMs. (l) Degradation performances of pollutants in the continuous Fe-SAC/CMs system.
(a-b) Reproduced with permission[152]. Copyright 2020, Springer Nature. (c-e) Reprinted with permission [59]. Copyright 2023, American Chemical Society. (f-g) Reproduced with permission [151]. Copyright 2024, Elsevier. (h-i) Reprinted with permission [160]. Copyright 2022, American Chemical Society. (j-l) Reproduced with permission[161]. Copyright 2024, National Academy of Science.

Compared with CMs, the water flux of Fe-SAC/CMs steadily decreased from 170 L m^{-2} h^{-1} to 152 L m^{-2} h^{-1}, and the higher and stable water flux was conducive to continuous water purification (Fig. 12k). And Fe-SAC/CMs has been shown to remove different simulated pollutants and multiple pollutants under environmental conditions through PMS activation (Fig. 12l). All these device-level demonstrations underline the practical application potential of SACs, emphasizing their high durability and activity.

In summary, catalytic activity increases with decreasing active center scale, but dual-atom catalysts or ultra-small cluster catalysts with sufficiently exposed active centers may exert better performance than SACs due to modulation of the electronic structure. In terms of catalytic selectivity, on the one hand, the diverse ligand structure of NPCs will lead to a variety of active species. While the active site of SACs is well-defined, the active species is usually single. On the other hand, the larger metal center scale usually possesses higher adsorption energy, which will lead to the O-O of the peroxides being elongated and more prone to break, so with the metal center ranging from small to large, the active species will show a tendency to be converted from non-radicals to radicals. In terms of catalytic stability, SACs typically exhibit lower leaching of metal ions and a slower decrease in catalytic activity due to stronger metal-carrier interactions.

4. Intrinsic mechanisms of structure-performance relationships from NPCs to SACs

The essential distinction between catalysis by SACs and NPCs is the influence of the coordination environment. The coordination environment and electronic structure of the metal active center have an essential influence on catalytic activity and mechanism leading to the activation of oxygen-containing components [118,162–167]. To intuitively observe the coordination difference between SACs and NPCs, X-ray absorption structure (XAS) analysis is employed. Single atoms are primarily coordinated by metal-X (M-X, where X = N, O, S, C…), while NPCs are dominated by metal-metal (M-M) coordination and auxiliary to M-X coordination [81]. Changes in the coordination structure inevitably lead to changes in the conformation of the adsorbed molecules, subsequently impacting the activity, selectivity, and stability of the reaction. Therefore, exploring the mechanism of Fenton-like catalysis at the atomic and electronic levels holds significant importance. However, the coordination in NPCs is diverse, and the complex diversity in the geometric and electronic structure of metal atoms makes it challenging to study the role of M-M coordination. Fortunately, the tunable synthesis of SACs provides a solution to this problem. During the synthesis of SACs, the distance between metal atoms can be changed by adjusting the amount of metal precursors added [168]. As displayed in Fig. 13, adjacent metal atoms are bound to each other in the first coordination shell or through non-metal atoms (e.g., N, S, and O) [45,169–171]. Multi-metal interactions occur when the metals are closer to each other. Moreover, when the distance between two metal atoms is close enough, significant electronic effects are induced by electron transfer between adjacent metal atoms [111,127,172]. This controlled synthesis of SACs provides valuable insights into the influence of coordination on catalytic

behavior at the atomic and electronic levels.

The local coordination environment of the metal center, specifically the coordination composition and coordination number, exerts significant control over their electronic structure, affecting orbital overlap and electron transfer. These factors decisively regulate the interaction of the active center with the adsorbent [173–178]. Studies showed that the intrinsic activity of PMS was activated by different metal centers (Co, Fe, Mn and Ni) from the perspective of spin states [179]. The large effective magnetic moment (μ_{eff}) with high spin states enhanced the degree of electron overlap between M 3d orbitals and O 2p orbitals. As shown in Fig. 14a, the high bonding strength accelerates the electron transfer rate and highlights the adsorption and activation of PMS activation. In addition, a positive correlation between •OH-induced oxidative activity and the d-band center on the M_1-N_4 site (M = Fe, Co, Ni, or Cu) has been revealed (Fig. 14b) [51]. The enhancement of the d-band center enhanced the strength of the interaction of the •OH intermediate with the M_1-N_4 site, thereby increasing the oxidative activity. Moreover, the impact of coordination number on catalytic performance and the mechanism of Fenton-like reactions has garnered attention [99,116,157, 180]. For example, an unsaturated coordination of a single-atom Co-N_3 catalyst, in contrast to a conventional Co-N_4 catalyst, was designed for PMS activation [116]. The electron density difference analysis illustrated the more robust electron transfer from Co-N_3 to PMS (Fig. 14c), which is an essential factor in promoting the transition from Co(II) to Co (IV), while the insufficient electron flow between Co-N_4 and PMS can only induce the cycle of Co(II)/Co(III) with radical generation (Fig. 14d). Furthermore, modifications of amino groups in modeled catalysts demonstrated the effect of electronic structure on Fenton-like reactions [154]. The modification of amino groups affects the charge distribution, resulting in a noticeably higher electron density of the metal center (Fig. 14e). Analysing the molecular orbitals, the change in the amino ligand led to a significant increase in the dz^2 orbitals compared to CoPc (Fig. 14f). As the energy gap between dz^2 and dxy increases, the binding energy of the dz^2 electrons decreases. Thus, CoPc-NH_2 is more likely to provide electrons and PMS is more likely to be activated. Besides, the positive shift of the d-band center led to a decreased occupation, which was beneficial for promoting the adsorption strength of PMS and the formation of *PMS as a key reaction intermediate (Fig. 14g). Moreover, electron-rich groups carried by pollutants can also modify the electronic structure of the active site [155]. The surface-confinement effect forming through the strong adsorption effect on pollutants can enhance the electron transfer between the catalyst and the PMS (Fig. 14h), which in turn improves the performance of Fenton-like reactions (Fig. 14i).

The broader implementation of SACs synthesis methods has led to promising advancements in creating catalysts with M-M coordination environments. Insufficient density results in completely isolated metal atoms without a distance effect, while excessive density leads to metal aggregation into large nanoparticles. Fe-Fe interactions changed the electronic structure and thus the catalytic mechanism (Fig. 15a) [111]. Moreover, Cheng et al. regulated the contents of Fe sites with different Fe-Fe distances by adjusting the Fe-atom loading (Fig. 15b) [115]. Fe sites with Fe-Fe distances of >5, 4–5, and <4 Å correspond to the models
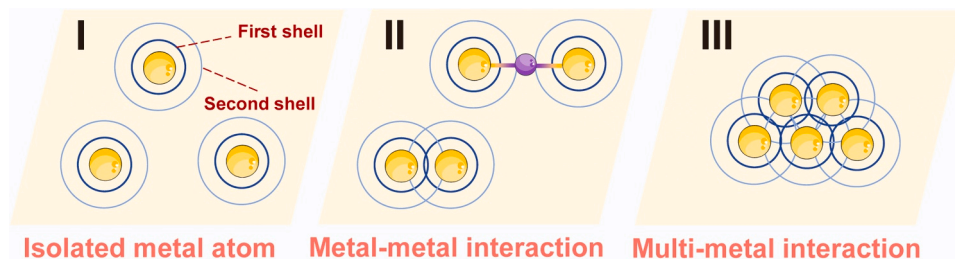

Fig. 13. Structural features of isolated metal atom (I), metal-metal interaction (II), and multi-metal interaction (III).
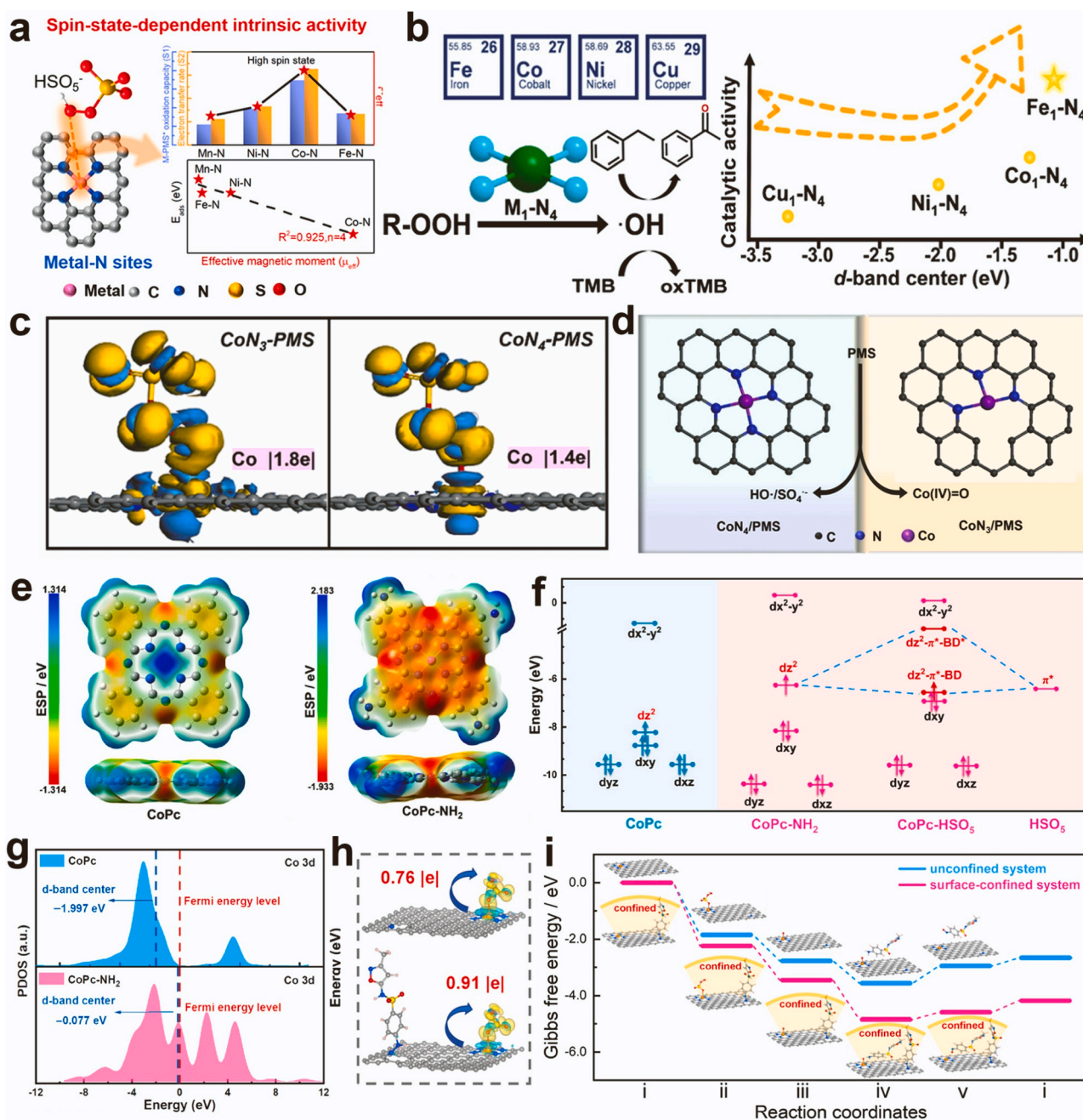
Fig. 14. (a) Correlation between E_{ads}, the experimental results and μ_{eff} ($p < 0.05$). (b) Correlation between the d-band center of M_1–N_4 sites and catalytic oxidation activity. (c) Electron density difference maps of Co-N_3-PMS (left) and Co-N_4-PMS (right), the light blue and yellow colors represent the electron depletion and electron accumulation, respectively. (d) The proposed reaction mechanism for activation of PMS by Co-N_3 and Co-N_4. (e) Molecular electrostatic potential of CoPc and CoPc-NH_2. (f) Energy levels of Co 3d orbital and orbital interactions between PMS and CoPc-NH_2. (g) Density-of-states of Co 3d in CoPc and CoPc-NH_2. (h) Electron density difference for FeSA-MNC and FeSA-MNC/SMX. (i) Reaction pathways of PMS activation at Fe−N_4 sites and the corresponding Gibbs free energy (eV). (a) Reprinted with permission [179]. Copyright 2021, American Chemical Society. (b) Reprinted with permission [51]. Copyright 2023, American Chemical Society. (c-d) Reproduced with permission [116]. Copyright 2023, Elsevier. (e-g) Reprinted with permission [154]. Copyright 2023, American Chemical Society. (h-i) Reprinted with permission [155]. Copyright 2023, American Chemical Society.

of Fe-N_4, 2Fe-N_4, and Fe$_2$-N_6, respectively. When PMS was adsorbed on 2Fe-N_4, a unique stable adsorption configuration was formed due to the well-matched size of the PMS molecule ($\sim$4.2 Å) and the Fe-Fe distance in 2Fe-N_4, which significantly enhanced the charge transfer (Fig. 15c). And the lower free energy change (ΔG) on 2Fe-N_4 relative to Fe$_2$-N_6 suggests that the thermodynamic conditions are more favorable to produce Fe^{IV}=O at this position (Fig. 15d). Similarly, site distance effect-induced two-site adsorption structure was also found in the study by Wang et al. in regulating the activation of PDS by Cu-Cu distance

(Fig. 15e) [112]. Besides, the synergistic effect of different metals (M_1-M_2) has also received attention [42,106,128,181]. Improving the electronic structure of the active center could be achieved through Fe-Co double-atom interactions [42]. The area ratio of L_3-edge and L_2-edge in Co and Fe L-edge XANES was positively correlated with the spin states, so the decrease of Co L_3/L_2 and the increase of Fe L_3/L_2 in FeCo-N/C indicated the change of the corresponding spin states (Fig. 15f). The μ_{eff}, also positively correlated with the spin state, further reflected the increase of the Co spin state and the decrease of the Fe spin state in
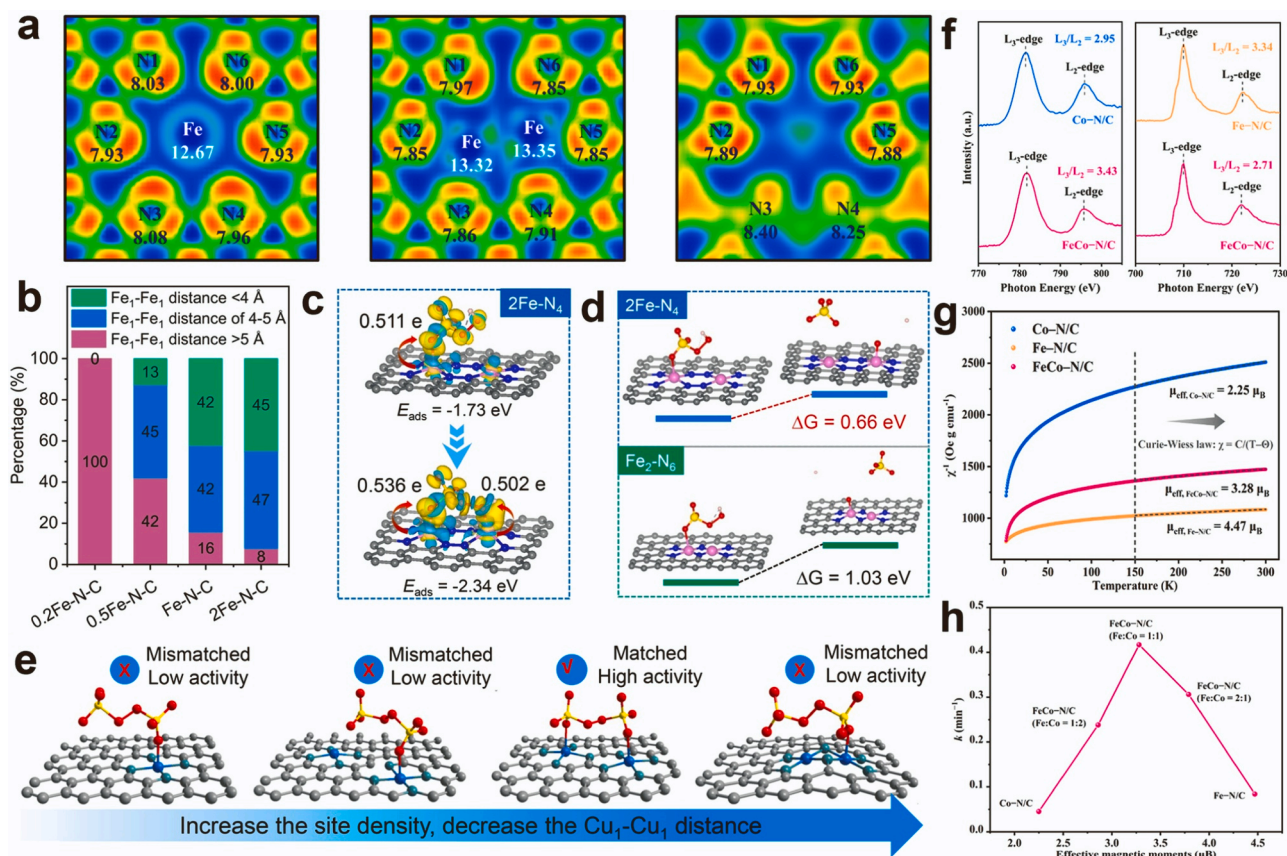
Fig. 15. (a) Electron localization function (ELF) maps and Bader charge calculation of Fe₁CN (left), Fe₂CN (middle), and FeₙCN (right). (b) Histogram of the contents of Fe atoms with different Fe-Fe distances. (c) The charge density difference for different PMS adsorption structures on the 2Fe-N₄ site. (d) Free energy changes for generating Fe^{IV}=O on 2Fe-N₄ and Fe₂-N₆ sites. (e) Depiction of Cu₁-Cu₁ distance manipulation for PDS adsorption and activation. (f) Co L-edge (left) and Fe L-edge (right) XANES spectra of Co-N/C, Fe-N/C, and FeCo-N/C. (g) Temperature-dependent magnetic susceptibilities of Co-N/C, Fe-N/C, and FeCo-N/C. (h) Relationship curve of reaction rate constants versus μ$_{eff}$ of different catalysts.

(a) Reprinted with permission [111]. Copyright 2022, American Chemical Society. (b-d) Reproduced with permission [115]. Copyright 2023, Wiley-VCH. (e) Reproduced with permission [112]. Copyright 2022, Wiley-VCH. (h) Reprinted with permission[42]. Copyright 2023, American Chemical Society.

FeCo-N/C (Fig. 15g). Fig. 15h revealed the relationship between the *k*-value and μ$_{eff}$ of the catalyst, FeCo-N/C with the medium spin state exhibiting the highest catalytic performance which corresponds to the calculated results.

At present, the research in active center size-dependent Fenton-like catalysis predominantly emphasizes the superior performance of SACs due to their high active site density compared to NPCs. However, limited attention has been given to the distinct performances arising from differences in their coordination environments. The lack of understanding regarding the nature of catalysis can lead to misinterpretations of the reaction mechanism. Even with identical coordination structures, disparate reaction mechanisms are reported in various articles. For example, in the investigation of PMS activation by the Co-N₄ active center, researchers have arrived at different conclusions regarding active species, including high-valent cobalt-oxo species, radicals, and ¹O₂ [157,182,183]. Several factors may contribute to this discrepancy: (1) potential deviations in parameters during XAS data fitting and DFT calculations, resulting in inaccurate exploration of the coordination structure; (2) the impact of different substrates on the electronic structure and orbital energy levels of the active center, influencing PMS adsorption and catalytic mechanisms; (3) the density of active sites affecting the distance between them, potentially altering interactions between adjacent active sites. Furthermore, M-M coordination enables the tuning of atomic structure, local coordination and electronic properties of single metal atoms. Thus, M-M coordination allows the tuning of local coordination and electronic properties of active centers, indicating that M-M coordination has the potential to exhibit superior

catalytic performance compared to M-X coordination [184,185]. While active site density is undoubtedly crucial for catalytic activity, understanding the performance differences between NPCs, NCCs, and SACs can guide the synthesis and application of advanced catalytic materials at the coordination and electronic structure levels.

5. Summary and outlook

In recent years, significant progress has been made in the application of heterogeneous catalysts in Fenton-like catalysis. The catalytic performance is notably sensitive to the scale and structure of the metal active center. SACs with atomically active sites have facilitated the exploration of structure-performance relationships, paving the way for the development of more advanced heterogeneous catalysts. In this comprehensive review, we delineate the synthetic regulation approaches from NPCs to NCCs, and to SACs. Moreover, the structure-performance relationships among NPCs, NCCs and SACs are also summarized in detail. The trends in catalytic activity, selectivity, and stability demonstrate enhancement as the active center scale decreases. However, an emerging body of research also indicates that M-M interactions or small nanoclusters exhibit superior catalytic performance. The alteration of the metal active center scale not only impacts catalytic activity but also introduces significant variations in catalytic selectivity and stability. Furthermore, the effects of the coordination environment between nanoparticles and single atoms on their performance are also summarized and prospected. Catalysts with M-M interaction show unique catalytic properties and become promising advanced catalysts

for Fenton-like catalysis. Benefiting from the modulation of activity, stability and reaction mechanisms, active center size-dependent catalysts show great potential for practical applications. Although substantial progress has been made in the regulation of active center scale, performance and mechanism exploration, the application of size-dependent catalysts in Fenton-like reactions is still in its infancy. Several essential challenges remain to be addressed to pave the way for the future development of advanced Fenton-like catalysts.

(1) **Precise regulation of active centers**

The accurate analysis of the mechanism relies on precise modulation of the coordination structure. In particular, synergistic size-dependent catalysts have shown excellent activity potential in recent years. The realization of interaction with single atom-single atom, single atom-cluster, and single atom-nanoparticle synergistic catalysis requires the support of precise catalytic site preparation. However, manipulating different sizes or coordination environments usually requires changing the synthesis conditions, such as doping heteroatoms precursor and controlling the calcination temperature. Changes in synthesis conditions will also impact the carrier, uneven carriers may result in inconsistent catalytic performance across individual metal central sites in SACs, leading to imprecise comparisons. In addition, the existing active site modulation methods have problems with uneven doping and the inability to regulate the active center precisely. Developing precise regulatory strategies for active sites is crucial for accurately determining the reaction mechanism and understanding structure-performance relationships at the molecular and atomic levels.

(2) **Development of emerging and in situ characterization techniques**

The identification of active sites and the exploration of the reaction mechanism are essential aspects of theoretical research. Limited characterization methods hinder the study of structure-performance relationships. For example, metal-metal interactions in SACs are challenging to discover by existing characterization methods. Underdeveloped characterization methods may mislead the DFT calculations and make the results inaccurate. Besides, catalytic reactions are dynamic processes in which the properties of the catalytic center change as the catalytic reaction proceeds. Currently, there is little experimental evidence for monitoring the dynamic behavior of SACs during catalysis. Achieving the discrimination of single-atom microenvironments under reaction conditions and monitoring the dynamic evolution of active centers during catalytic reactions in real time is exceptionally challenging. Therefore, developing new characterization methods and in situ characterization techniques with atomic resolution will meaningfully facilitate the study of catalytic mechanisms. In addition, theoretical simulations based on machine learning should also receive more attention.

(3) **Pay more attention to the role of carrier**

The same coordination structure existed in different studies, but different mechanisms have been proposed, resulting from the poor understanding of the nature of catalysis. In many cases, a single metal atom may not solely determine the catalytic reaction. The carrier material, the surrounding coordination atom and even other substances in the dissolution (such as pollutants and oxidants) play an extremely important and even decisive role. Support materials, such as carbon or other metals, have outstanding effects in Fenton-like catalysis, especially for activating PMS. Despite this, many studies focus only on the role of active metal centers, overlooking the effect of supports on catalytic activity. Therefore, more attention should be paid to the role of the carrier in exploring the nature of catalysis.

(4) **Industrial applications**

Industrial applications require the development of catalysts with stability as well as high activity. SACs, NCCs and NPCs have their advantages, e.g., SACs produce mainly non-radical active species, which are advantageous in the selective degradation of electron-rich pollutants; while NPCs usually produce highly reactive radicals, which are advantageous in the degradation of electron-deficient pollutants. In considering practical applications, their respective advantages should be utilized or combined to cater for different practical applications. Besides, the mechanical strength of columnar and membrane Fenton filters has not received sufficient attention. Moreover, catalyst "poisoning" is widespread in Fenton-like reactions, and regeneration of catalysts often requires high-temperature treatment increasing the cost of practical applications. Therefore, improving the activity and stability of SACs is crucial for meeting the requirements of long and stable industrial operations

CRediT authorship contribution statement

Xinhao Wang: Formal analysis. **Hongyu Zhou:** Writing – review & editing. **Zelin Wu:** Conceptualization. **Bingkun Huang:** Writing – review & editing, Writing – original draft, Investigation, Formal analysis, Conceptualization. **Bo Lai:** Writing – review & editing, Supervision, Conceptualization. **Zhaokun Xiong:** Writing – review & editing, Visualization, Supervision, Funding acquisition, Formal analysis, Conceptualization. **Heng Zhang:** Conceptualization. **Yang Liu:** Supervision.

Declaration of Competing Interest

The authors declare that they have no known competing financial interests or personal relationships that could have appeared to influence the work reported in this paper.

Data Availability

Data will be made available on request.

Acknowledgements

Appendix A. Supporting information

Supplementary data associated with this article can be found in the online version at doi:10.1016/j.apcatb.2024.124157.

References

[1] M.A. Shannon, P.W. Bohn, M. Elimelech, J.G. Georgiadis, B.J. Marinas, A. M. Mayes, Science and technology for water purification in the coming decades, Nature 452 (2008) 301–310.

[2] Y. Xu, Z. Mao, R. Qu, J. Wang, J. Yu, X. Luo, M. Shi, X. Mao, J. Ding, B. Liu, Electrochemical hydrogenation of oxidized contaminants for water purification without supporting electrolyte, Nat. Water 1 (2023) 95–103.

[3] W.H. Glaze, J.-W. Kang, D.H. Chapin, The chemistry of water treatment processes involving ozone, hydrogen peroxide and ultraviolet radiation, Ozone-Sci. Eng. 9 (1987) 335–352.

[4] X. Wu, J.-H. Kim, Outlook on Single Atom Catalysts for Persulfate-Based Advanced Oxidation, ACS EST Engg 2 (2022) 1776–1796.

[5] Y. Long, J. Dai, S. Zhao, Y. Su, Z. Wang, Z. Zhang, Atomically dispersed cobalt sites on graphene as efficient periodate activators for selective organic pollutant degradation, Environ. Sci. Technol. 55 (2021) 5357–5370.

[6] L.-Z. Huang, X. Wei, E. Gao, C. Zhang, X.-M. Hu, Y. Chen, Z. Liu, N. Finck, J. Lützenkirchen, D.D. Dionysiou, Single Fe atoms confined in two-dimensional MoS$_2$ for sulfite activation: a biomimetic approach towards efficient radical generation, Appl. Catal. B 268 (2020) 118459.

[7] Z. Wu, Y. Wang, Z. Xiong, Z. Ao, S. Pu, G. Yao, B. Lai, Core-shell magnetic Fe₃O₄@Zn/Co-ZIFs to activate peroxymonosulfate for highly efficient degradation of carbamazepine, Appl. Catal. B 277 (2020) 119136.

[8] Z. Wu, Z. Xiong, R. Liu, C. He, Y. Liu, Z. Pan, G. Yao, B. Lai, Pivotal roles of N-doped carbon shell and hollow structure in nanoreactor with spatial confined Co species in peroxymonosulfate activation: obstructing metal leaching and enhancing catalytic stability, J. Hazard. Mater. 427 (2022) 128204.

[9] Z. Wang, W. Wang, J. Wang, Y. Yuan, Q. Wu, H. Hu, High-valent iron-oxo species mediated cyclic oxidation through single-atom Fe-N6 sites with high peroxymonosulfate utilization rate, Appl. Catal. B 305 (2022) 121049.

[10] B. Huang, Z. Xiong, P. Zhou, H. Zhang, Z. Pan, G. Yao, B. Lai, Ultrafast degradation of contaminants in a trace cobalt(II) activated peroxymonosulfate process triggered through borate: Indispensable role of intermediate complex, J. Hazard. Mater. 424 (2022) 127641.

[11] X. Long, Z. Xiong, R. Huang, Y. Yu, P. Zhou, H. Zhang, G. Yao, B. Lai, Sustainable Fe(III)/Fe(II) cycles triggered by co-catalyst of weak electrical current in Fe(III)/peroxymonosulfate system: collaboration of radical and non-radical mechanisms, Appl. Catal. B 317 (2022) 121716.

[12] Y. Hong, H. Zhou, Z. Xiong, Y. Liu, G. Yao, B. Lai, Heterogeneous activation of peroxymonosulfate by CoMgFe-LDO for degradation of carbamazepine: efficiency, mechanism and degradation pathways, Chem. Eng. J. 391 (2020) 123604.

[13] Z. Xiong, Y. Jiang, Z. Wu, G. Yao, B. Lai, Synthesis strategies and emerging mechanisms of metal-organic frameworks for sulfate radical-based advanced oxidation process: A review, Chem. Eng. J. 421 (2021) 127863.

[14] Y. Yu, Z. Xiong, B. Huang, X. Wang, Y. Du, C. He, Y. Liu, G. Yao, B. Lai, Synchronous removal of pharmaceutical contaminants and inactivation of pathogenic microorganisms in real hospital wastewater by electro-peroxone process, Environ. Int. 168 (2022) 107453.

[15] R. Zhang, M. Chen, Z. Xiong, Y. Guo, B. Lai, Highly efficient degradation of emerging contaminants by magnetic CuO@FexOy derived from natural mackinawite (FeS) in the presence of peroxymonosulfate, Chin. Chem. Lett. 33 (2022) 948–952.

[16] Y. Jiang, Z. Xiong, J. Huang, F. Yan, G. Yao, B. Lai, Effective E. coli inactivation of core-shell ZnO@ZIF-8 photocatalysis under visible light synergize with peroxymonosulfate: efficiency and mechanism, Chin. Chem. Lett. 33 (2022) 415–423.

[17] A. Han, B. Wang, A. Kumar, Y. Qin, J. Jin, X. Wang, C. Yang, B. Dong, Y. Jia, J. Liu, X. Sun, Recent Advances for MOF-Derived Carbon-Supported Single-Atom Catalysts, Small, Methods 3 (2019) 1800471.

[18] Z. Li, D. Wang, Y. Wu, Y. Li, Recent advances in the precise control of isolated single-site catalysts by chemical methods, Natl. Sci. Rev. 5 (2018) 673–689.

[19] A. Wang, J. Li, T. Zhang, Heterogeneous single-atom catalysis, Nat. Rev. Chem. 2 (2018) 65–81.

[20] G. Giannakakis, S. Mitchell, J. Pérez-Ramírez, Single-atom heterogeneous catalysts for sustainable organic synthesis, Trends Chem. 4 (2022) 264–276.

[21] L. Jiao, H. Yan, Y. Wu, W. Gu, C. Zhu, D. Du, Y. Lin, When Nanozymes Meet Single-Atom, Catal., Angew. Chem. Int. Ed. 59 (2020) 2565–2576.

[22] L. Liu, A. Corma, Metal Catalysts for Heterogeneous Catalysis: From Single Atoms to Nanoclusters and Nanoparticles, Chem. Rev. 118 (2018) 4981–5079.

[23] F. Doherty, H. Wang, M. Yang, B.R. Goldsmith, Nanocluster and single-atom catalysts for thermocatalytic conversion of CO and CO₂, Catal. Sci. Technol. 10 (2020) 5772–5791.

[24] J. Liu, Catalysis by Supported Single Metal Atoms, ACS Catal. 7 (2016) 34–59.

[25] H. Zhang, W. Tian, X. Duan, H. Sun, S. Liu, S. Wang, Catalysis of a Single Transition Metal Site for Water Oxidation: From Mononuclear Molecules to Single Atoms, Adv. Mater. 32 (2020) 1904037.

[26] B. Qiao, A. Wang, X. Yang, L.F. Allard, Z. Jiang, Y. Cui, J. Liu, J. Li, T. Zhang, Single-atom catalysis of CO oxidation using Pt₁/FeOₓ, Nat. Chem. 3 (2011) 634–641.

[27] Y. Xiong, W. Sun, P. Xin, W. Chen, X. Zheng, W. Yan, L. Zheng, J. Dong, J. Zhang, D. Wang, Y. Li, Gram-Scale Synthesis of High-Loading Single-Atomic-Site Fe Catalysts for Effective Epoxidation of Styrene, Adv. Mater. 32 (2020) 2000896.

[28] Y. Cheng, S. He, S. Lu, J.P. Veder, B. Johannessen, L. Thomsen, M. Saunders, T. Becker, R. De Marco, Q. Li, S.Z. Yang, S.P. Jiang, Iron single atoms on graphene as nonprecious metal catalysts for high-temperature polymer electrolyte membrane fuel cells, Adv. Sci. 6 (2019) 1802066.

[29] C. Tang, L. Chen, H. Li, L. Li, Y. Jiao, Y. Zheng, H. Xu, K. Davey, S.Z. Qiao, Tailoring acidic oxygen reduction selectivity on single-atom catalysts via modification of first and second coordination spheres, J. Am. Chem. Soc. 143 (2021) 7819–7827.

[30] S. Zuo, X. Jin, X. Wang, Y. Lu, Q. Zhu, J. Wang, W. Liu, Y. Du, J. Wang, Sandwich structure stabilized atomic Fe catalyst for highly efficient Fenton-like reaction at all pH values, Appl. Catal. B 282 (2021) 119551.

[31] N. Du, Y. Liu, Q. Li, W. Miao, D. Wang, S. Mao, Peroxydisulfate activation by atomically-dispersed Fe-Nx on N-doped carbon: mechanism of singlet oxygen evolution for nonradical degradation of aqueous contaminants, Chem. Eng. J. (2020) 127545.

[32] Z. Zhao, W. Zhang, W. Liu, Y. Li, J. Ye, J. Liang, M. Tong, Activation of sulfite by single-atom Fe deposited graphitic carbon nitride for diclofenac removal: The synergetic effect of transition metal and photocatalysis, Chem. Eng. J. 407 (2021) 127167.

[33] L. Yang, H. Yang, S. Yin, X. Wang, M. Xu, G. Lu, Z. Liu, H. Sun, Fe Single-Atom Catalyst for Efficient and Rapid Fenton-Like Degradation of Organics and Disinfection against Bacteria, Small 18 (2022) 2104941.

[34] L. Su, P. Wang, X. Ma, J. Wang, S. Zhan, Regulating Local Electron Density of Iron Single Sites by Introducing Nitrogen Vacancies for Efficient Photo-Fenton Process, Angew. Chem. Int. Ed. 60 (2021) 21261–21266.

[35] Y. Shang, X. Duan, S. Wang, Q. Yue, B. Gao, X. Xu, Carbon-based single atom catalyst: Synthesis, characterization, DFT calculations, Chin. Chem. Lett. 33 (2022) 663–673.

[36] Z. Zhao, H. Tan, P. Zhang, X. Liang, T. Li, Y. Gao, C. Hu, Turning the inert element zinc into an active single-atom catalyst for efficient fenton-like chemistry, Angew. Chem. Int. Ed. (2023) e202219178.

[37] Y. Gao, B. Liu, D. Wang, Microenvironment engineering of single/dual-atom catalysts for electrocatalytic application, Adv. Mater. (2023) e2209654.

[38] Z. Wu, B. Huang, X. Wang, C.-S. He, Y. Liu, Y. Du, W. Liu, Z. Xiong, B. Lai, Facilely tuning the first-shell coordination microenvironment in iron single-atom for fenton-like chemistry toward highly efficient wastewater purification, Environ. Sci. Technol. 57 (2023) 14046–14057.

[39] F. Mo, C. Song, Q. Zhou, W. Xue, S. Ouyang, Q. Wang, Z. Hou, S. Wang, J. Wang, The optimized Fenton-like activity of Fe single-atom sites by Fe atomic clusters-mediated electronic configuration modulation, Proc. Natl. Acad. Sci. U. S. A. 120 (2023) e2300281120.

[40] S. An, G. Zhang, T. Wang, W. Zhang, K. Li, C. Song, J.T. Miller, S. Miao, J. Wang, X. Guo, High-Density Ultra-small Clusters and Single-Atom Fe Sites Embedded in Graphitic Carbon Nitride (g-C₃N₄) for Highly Efficient Catalytic Advanced Oxidation Processes, ACS Nano 12 (2018) 9441–9450.

[41] L. Peng, X. Duan, Y. Shang, B. Gao, X. Xu, Engineered carbon supported single iron atom sites and iron clusters from Fe-rich Enteromorpha for Fenton-like reactions via nonradical pathways, Appl. Catal. B 287 (2021) 119963.

[42] Z. Zhao, M. Hu, T. Nie, W. Zhou, B. Pan, B. Xing, L. Zhu, Improved Electronic Structure from Spin-State Reconstruction of a Heteronuclear Fe-Co Diatomic Pair to Boost the Fenton-like Reaction, Environ. Sci. Technol. 57 (2023) 4556–4567.

[43] Z. Chen, F. An, Y. Zhang, Z. Liang, W. Liu, M. Xing, Single-atom Mo–Co catalyst with low biotoxicity for sustainable degradation of high-ionization-potential organic pollutants, Proc. Natl. Acad. Sci. U. S. A. 120 (2023) e2305933120.

[44] L. Liu, Y. Chen, S. Li, W. Yu, X. Zhang, H. Wang, J. Ren, Z. Bian, Enhanced electrocatalytic cathodic degradation of 2,4-dichlorophenoxyacetic acid based on a synergistic effect derived from Co single atoms and Cu nanoclusters, Appl. Catal. B 332 (2023) 122748.

[45] X. Wang, S. Qiu, J. Feng, Y. Tong, F. Zhou, Q. Li, L. Song, S. Chen, K.H. Wu, P. Su, S. Ye, F. Hou, S.X. Dou, H.K. Liu, G.Q. Max Lu, C. Sun, J. Liu, J. Liang, Confined Fe-Cu Clusters as Sub-Nanometer Reactors for Efficiently Regulating the Electrochemical Nitrogen Reduction Reaction, Adv. Mater. 32 (2020) 2004382.

[46] H. Qi, J. Yang, F. Liu, L. Zhang, J. Yang, X. Liu, L. Li, Y. Su, Y. Liu, R. Hao, A. Wang, T. Zhang, Highly selective and robust single-atom catalyst Ru₁/NC for reductive amination of aldehydes/ketones, Nat. Commun. 12 (2021) 3295.

[47] L. Nie, D. Mei, H. Xiong, B. Peng, Z. Ren, X.I.P. Hernandez, A. DeLaRiva, M. Wang, M.H. Engelhard, L. Kovarik, A.K. Datye, Y. Wang, Activation of surface lattice oxygen in single-atom Pt/CeO₂ for low-temperature CO oxidation, Science 358 (2017) 1419–1423.

[48] L. Wen, K. Sun, X. Liu, W. Yang, L. Li, H.L. Jiang, Electronic State and Microenvironment Modulation of Metal Nanoparticles Stabilized by MOFs for Boosting Electrocatalytic Nitrogen Reduction, Adv. Mater. 35 (2023) e2210669.

[49] T. Tang, Z. Wang, J. Guan, Optimizing the electrocatalytic selectivity of carbon dioxide reduction reaction by regulating the electronic structure of single-atom M-N-C materials, Adv. Funct. Mater. 32 (2022) 2111504.

[50] B. Han, Y. Luo, Y. Lin, B. Weng, D. Xia, Y. Zhou, C. Guan, Z. Wang, X. Wei, J. Jiang, Microenvironment engineering of single-atom catalysts for persulfate-based advanced oxidation processes, Chem. Eng. J. 447 (2022) 137551.

[51] J. Duan, Y. Zhou, Y. Ren, F. Liu, P. Deng, M. Yang, H. Ge, J. Gao, J. Yang, Y. Qin, Effect of Electronic Structure over Late Transition-Metal M1–N₄ Single-Atom Sites on Hydroxyl Radical-Induced Oxidations, ACS Catal. 13 (2023) 3308–3316.

[52] X. Ren, J. Zhao, X. Li, J. Shao, B. Pan, A. Salamé, E. Boutin, T. Groizard, S. Wang, J. Ding, X. Zhang, W.-Y. Huang, W.-J. Zeng, C. Liu, Y. Li, S.-F. Hung, Y. Huang, M. Robert, B. Liu, In-situ spectroscopic probe of the intrinsic structure feature of single-atom center in electrochemical CO/CO₂ reduction to methanol, Nat. Commun. 14 (2023) 3401.

[53] B. Huang, Z. Wu, H. Zhou, J. Li, C. Zhou, Z. Xiong, Z. Pan, G. Yao, B. Lai, Recent advances in single-atom catalysts for advanced oxidation processes in water purification, J. Hazard. Mater. 412 (2021) 125253.

[54] Y. Shang, X. Xu, B. Gao, S. Wang, X. Duan, Single-atom catalysis in advanced oxidation processes for environmental remediation, Chem. Soc. Rev. 50 (2021) 5281–5322.

[55] P. Xia, C. Wang, Q. He, Z. Ye, I. Sirés, MOF-derived single-atom catalysts: The next frontier in advanced oxidation for water treatment, Chem. Eng. J. 452 (2023) 139446.

[56] W. Qu, C. Chen, Z. Tang, H. Wen, L. Hu, D. Xia, S. Tian, H. Zhao, C. He, D. Shu, Progress in metal-organic-framework-based single-atom catalysts for environmental remediation, Coord. Chem. Rev. 474 (2023) 214855.

[57] L. Hao, C. Guo, Z. Hu, R. Guo, X. Liu, Y. Tian, Single-atom catalysts based on Fenton-like/peroxymonosulfate system for water purification: design and synthesis principle, performance regulation and catalytic mechanism, Nanoscale 14 (2022) 13861–13889.

[58] X. Han, X. Ling, Y. Wang, T. Ma, C. Zhong, W. Hu, Y. Deng, Generation of nanoparticle, atomic-cluster, and single-atom cobalt catalysts from zeolitic imidazole frameworks by spatial isolation and their use in zinc-air batteries, Angew. Chem. Int. Ed. 58 (2019) 5359–5364.

[59] Z. Wu, Z. Xiong, W. Liu, R. Liu, X. Feng, B. Huang, X. Wang, Y. Gao, H. Chen, G. Yao, B. Lai, Active center size-dependent fenton-like chemistry for sustainable water decontamination, Environ. Sci. Technol. 57 (2023) 21416–21427.

[60] Y. Yao, C. Wang, X. Yan, H. Zhang, C. Xiao, J. Qi, Z. Zhu, Y. Zhou, X. Sun, X. Duan, J. Li, Rational Regulation of Co-N-C coordination for high-efficiency generation of $^1O_2$ toward nearly 100% selective degradation of organic pollutants, Environ. Sci. Technol. 56 (2022) 8833–8843.

[61] X. Wang, Z. Xiong, H. Shi, Z. Wu, B. Huang, H. Zhang, P. Zhou, Z. Pan, W. Liu, B. Lai, Switching the reaction mechanisms and pollutant degradation routes through active center size-dependent Fenton-like catalysis, Appl. Catal. B 329 (2023) 122569.

[62] Y. Yin, L. Shi, W. Li, X. Li, H. Wu, Z. Ao, W. Tian, S. Liu, S. Wang, H. Sun, Boosting Fenton-Like Reactions via Single Atom Fe Catalysis, Environ. Sci. Technol. 53 (2019) 11391–11400.

[63] C. Chu, D. Huang, S. Gupta, S. Weon, J. Niu, E. Stavitski, C. Muhich, J.H. Kim, Neighboring Pd single atoms surpass isolated single atoms for selective hydrodehalogenation catalysis, Nat. Commun. 12 (2021) 5179.

[64] X. Zhao, Y. Sun, J. Wang, A. Nie, G. Zou, L. Ren, J. Wang, Y. Wang, C. Fernandez, Q. Peng, Regulating d-Orbital Hybridization of Subgroup-IVB Single Atoms for Efficient Oxygen Reduction Reaction, Adv. Mater. (2024) 2312117.

[65] Z. Li, K. Li, S. Ma, B. Dang, Y. Li, H. Fu, J. Du, Q. Meng, Activation of peroxymonosulfate by iron-biochar composites: Comparison of nanoscale Fe with single-atom Fe, J. Colloid Interf. Sci. 582 (2021) 598–609.

[66] L. Zhang, Y. Jia, G. Gao, X. Yan, N. Chen, J. Chen, M.T. Soo, B. Wood, D. Yang, A. Du, X. Yao, Graphene defects trap atomic Ni species for hydrogen and oxygen evolution reactions, Chem 4 (2018) 285–297.

[67] J. Liu, J. Liao, K. Huang, J. Dong, G. He, Z. Gong, H. Fei, A General Strategy to Remove Metal Aggregates toward Metal-Nitrogen-Carbon Catalysts with Exclusive Atomic Dispersion, Adv. Mater. (2023) e2211398.

[68] W. Guo, Z. Wang, X. Wang, Y. Wu, General Design Concept for Single-Atom Catalysts toward Heterogeneous Catalysis, Adv. Mater. (2021) 2004287.

[69] T. Huang, L. Liu, J. Tao, L. Zhou, S. Zhang, Microbial fuel cells coupling with the three-dimensional electro-Fenton technique enhances the degradation of methyl orange in the wastewater, Environ. Sci. Pollut. Res. 25 (2018) 17989–18000.

[70] K. Huang, L. Zhang, T. Xu, H. Wei, R. Zhang, X. Zhang, B. Ge, M. Lei, J.Y. Ma, L. M. Liu, H. Wu, −60 °C solution synthesis of atomically dispersed cobalt electrocatalyst with superior performance, Nat. Commun. 10 (2019) 606.

[71] W. Zhong, W. Tu, Z. Wang, Z. Lin, A. Xu, X. Ye, D. Chen, B. Xiao, Ultralow-temperature assisted synthesis of single platinum atoms anchored on carbon nanotubes for efficiently electrocatalytic acidic hydrogen evolution, J. Energy Chem. 51 (2020) 280–284.

[72] H. Wei, K. Huang, D. Wang, R. Zhang, B. Ge, J. Ma, B. Wen, S. Zhang, Q. Li, M. Lei, C. Zhang, J. Irawan, L.M. Liu, H. Wu, Iced photochemical reduction to synthesize atomically dispersed metals by suppressing nanocrystal growth, Nat. Commun. 8 (2017) 1490.

[73] H. Wei, H. Wu, K. Huang, B. Ge, J. Ma, J. Lang, D. Zu, M. Lei, Y. Yao, W. Guo, H. Wu, Ultralow-temperature photochemical synthesis of atomically dispersed Pt catalysts for the hydrogen evolution reaction, Chem. Sci. 10 (2019) 2830–2836.

[74] R. Lang, W. Xi, J.C. Liu, Y.T. Cui, T. Li, A.F. Lee, F. Chen, Y. Chen, L. Li, L. Li, J. Lin, S. Miao, X. Liu, A.Q. Wang, X. Wang, J. Luo, B. Qiao, J. Li, T. Zhang, Non defect-stabilized thermally stable single-atom catalyst, Nat. Commun. 10 (2019) 234.

[75] W. Liu, H. Zhang, C. Li, X. Wang, J. Liu, X. Zhang, Non-noble metal single-atom catalysts prepared by wet chemical method and their applications in electrochemical water splitting, J. Energy Chem. 47 (2020) 333–345.

[76] A. Bruix, Y. Lykhach, I. Matolinova, A. Neitzel, T. Skala, N. Tsud, M. Vorokhta, V. Stetsovych, K. Sevcikova, J. Myslivecek, R. Fiala, M. Vaclavu, K.C. Prince, S. Bruyere, V. Potin, F. Illas, V. Matolin, J. Libuda, K.M. Neyman, Maximum noble-metal efficiency in catalytic materials: atomically dispersed surface platinum, Angew. Chem. Int. Ed. 53 (2014) 10525–10530.

[77] J. Zhang, X. Wu, W.C. Cheong, W. Chen, R. Lin, J. Li, L. Zheng, W. Yan, L. Gu, C. Chen, Q. Peng, D. Wang, Y. Li, Cation vacancy stabilization of single-atomic-site $Pt_1/Ni(OH)_x$ catalyst for diboration of alkynes and alkenes, Nat. Commun. 9 (2018) 1002.

[78] P. Yin, T. Yao, Y. Wu, L. Zheng, Y. Lin, W. Liu, H. Ju, J. Zhu, X. Hong, Z. Deng, G. Zhou, S. Wei, Y. Li, Single cobalt atoms with precise N-coordination as superior oxygen reduction reaction, Catal., Angew. Chem. Int. Ed. 55 (2016) 10800–10805.

[79] Y. Chen, S. Ji, Y. Wang, J. Dong, W. Chen, Z. Li, R. Shen, L. Zheng, Z. Zhuang, D. Wang, Y. Li, Isolated single iron atoms anchored on N-doped porous carbon as an efficient electrocatalyst for the oxygen reduction reaction, Angew. Chem. Int. Ed. 56 (2017) 6937–6941.

[80] J. Wang, G. Han, L. Wang, L. Du, G. Chen, Y. Gao, Y. Ma, C. Du, X. Cheng, P. Zuo, G. Yin, ZIF-8 with ferrocene encapsulated: a promising precursor to single-atom Fe embedded nitrogen-doped carbon as highly efficient catalyst for oxygen electroreduction, Small 14 (2018) 1704282.

[81] M.X. Gu, L.P. Gao, S.S. Peng, S.C. Qi, X.B. Shao, X.Q. Liu, L.B. Sun, Transition Metal Single Atoms Constructed by Using Inherent Confined Space, ACS Nano, (2023).

[82] X. He, Y. Deng, Y. Zhang, Q. He, D. Xiao, M. Peng, Y. Zhao, H. Zhang, R. Luo, T. Gan, H. Ji, D. Ma, Mechanochemical kilogram-scale synthesis of noble metal single-atom catalysts, Cell Rep. Phys. Sci. 1 (2020) 100004.

[83] T. Gan, Q. He, H. Zhang, H. Xiao, Y. Liu, Y. Zhang, X. He, H. Ji, Unveiling the kilogram-scale gold single-atom catalysts via ball milling for preferential oxidation of CO in excess hydrogen, Chem. Eng. J. 389 (2020) 124490.

[84] S. Sun, G. Zhang, N. Gauquelin, N. Chen, J. Zhou, S. Yang, W. Chen, X. Meng, D. Geng, M.N. Banis, R. Li, S. Ye, S. Knights, G.A. Botton, T.-K. Sham, X. Sun, Single-atom Catalysis Using Pt/Graphene Achieved through Atomic Layer Deposition, Sci. Rep. 3 (2013) 1775.

[85] S. Wei, A. Li, J.C. Liu, Z. Li, W. Chen, Y. Gong, Q. Zhang, W.C. Cheong, Y. Wang, L. Zheng, H. Xiao, C. Chen, D. Wang, Q. Peng, L. Gu, X. Han, J. Li, Y. Li, Direct observation of noble metal nanoparticles transforming to thermally stable single atoms, Nat. Nanotechnol. 13 (2018) 856–861.

[86] B. Elder, R. Neupane, E. Tokita, U. Ghosh, S. Hales, Y.L. Kong, Nanomaterial Patterning in 3D Printing, Adv. Mater. 32 (2020) e1907142.

[87] H. Yuk, B. Lu, S. Lin, K. Qu, J. Xu, J. Luo, X. Zhao, 3D printing of conducting polymers, Nat. Commun. 11 (2020) 1604.

[88] D. Wang, T. Zhi, L. Liu, L. Yan, W. Wan, Y. Tang, B. He, L. Hu, C. Jing, G. Jiang, 3D printing of TiO2 nano particles containing macrostructures for As(III) removal in water, Sci. Total. Environ. 815 (2022) 152754.

[89] F. Xie, X. Cui, X. Zhi, D. Yao, B. Johannessen, T. Lin, J. Tang, T.B.F. Woodfield, L. Gu, S.-Z. Qiao, A general approach to 3D-printed single-atom catalysts, Nat. Synth. 2 (2023) 129–139.

[90] L. Tian, X. Gao, S. Wang, C. Chen, M. Chen, W. Guo, Z. Wang, X. Tai, X. Han, C. Xu, Y. Ruan, M. Zhu, C. Xiong, T. Yao, H. Zhou, Y. Lin, Y. Wu, Precise arrangement of metal atoms at the interface by a thermal printing strategy, Proc. Natl. Acad. Sci. U. S. A. 120 (2023) e2310916120.

[91] Y. Gao, C. Yang, M. Zhou, C. He, S. Cao, Y. Long, S. Li, Y. Lin, P. Zhu, C. Cheng, Transition Metal and Metal-Nx Codoped MOF-derived fenton-like catalysts: a comparative study on single atoms and nanoparticles, Small 16 (2020) 2005060.

[92] H.-Z. Liu, X.-X. Shu, M. Huang, B.-B. Wu, J.-J. Chen, X.-S. Wang, H.-L. Li, H.-Q. Yu, Tailoring d-band center of high-valent metal-oxo species for pollutant removal via complete polymerization, Nat. Commun. 15 (2024) 2327.

[93] Y. Li, T. Yang, S. Qiu, W. Lin, J. Yan, S. Fan, Q. Zhou, Uniform N-coordinated single-atomic iron sites dispersed in porous carbon framework to activate PMS for efficient BPA degradation via high-valent iron-oxo species, Chem. Eng. J. 389 (2020) 124382.

[94] Y. Chen, J. Lin, B. Jia, X. Wang, S. Jiang, T. Ma, Isolating Single and Few Atoms for Enhanced Catalysis, Adv. Mater. 34 (2022) e2201796.

[95] C.X. Zhao, B.Q. Li, J.N. Liu, Q. Zhang, Intrinsic electrocatalytic activity regulation of M-N-C single-atom catalysts for the oxygen reduction reaction, Angew. Chem. Int. Ed. 60 (2021) 4448–4463.

[96] Y. Gao, X. Duan, B. Li, Q. Jia, Y. Li, X. Fan, F. Zhang, G. Zhang, S. Wang, W. Peng, Fe containing template derived atomic Fe–N–C to boost Fenton-like reaction and charge migration analysis on highly active Fe–N4 sites, J. Mater. Chem. A 9 (2021) 14793–14805.

[97] F. Li, Z. Lu, T. Li, P. Zhang, C. Hu, Origin of the Excellent Activity and Selectivity of a Single-Atom Copper Catalyst with Unsaturated Cu-N2 Sites via Peroxydisulfate Activation: Cu(III) as a Dominant Oxidizing Species, Environ. Sci. Technol. (2022) 8765–8775.

[98] Y. Gao, Y. Zhu, T. Li, Z. Chen, Q. Jiang, Z. Zhao, X. Liang, C. Hu, Unraveling the High-Activity Origin of Single-Atom Iron Catalysts for Organic Pollutant Oxidation via Peroxymonosulfate Activation, Environ. Sci. Technol. 55 (2021) 8318–8328.

[99] C. Zhu, C. Nie, F. Cun, Y. Wang, Z. Tian, F. Liu, Two-step pyrolysis to anchor ultrahigh-density single-atom FeN5 sites on carbon nitride for efficient Fenton-like catalysis near 0 °C, Appl. Catal. B 319 (2022) 121900.

[100] P. Duan, J. Pan, W. Du, Q. Yue, B. Gao, X. Xu, Activation of peroxymonosulfate via mediated electron transfer mechanism on single-atom Fe catalyst for effective organic pollutants removal, Appl. Catal. B 299 (2021) 120714.

[101] Y. Qi, J. Li, Y. Zhang, Q. Cao, Y. Si, Z. Wu, M. Akram, X. Xu, Novel lignin-based single atom catalysts as peroxymonosulfate activator for pollutants degradation: Role of single cobalt and electron transfer pathway, Appl. Catal. B 286 (2021) 119910.

[102] C. Dong, Z.-Q. Wang, C. Yang, X. Hu, P. Wang, X.-Q. Gong, L. Lin, X.-Y. Li, Sequential electrocatalysis by single molybdenum atoms/clusters doped on carbon nanotubes for removing organic contaminants from wastewater, Appl. Catal. B 338 (2023) 123060.

[103] J. Li, H. Xu, Z. Huang, Q. Hong, Y. Qiu, N. Yan, Z. Qu, Strengthen the Affinity of Element Mercury on the Carbon-Based Material by Adjusting the Coordination Environment of Single-Site Manganese, Environ. Sci. Technol. 55 (2021) 14126–14135.

[104] Y. Yao, J. Yang, C. Zhu, L. Lu, Q. Fang, C. Xu, Z. He, S. Song, Y. Shen, Unveiling the metallic size effect on O2 adsorption and activation for enhanced electro-Fenton degradation of aromatic compounds, J. Hazard. Mater. 462 (2024) 132739.

[105] J. Pan, B. Gao, P. Duan, K. Guo, M. Akram, X. Xu, Q. Yue, Y. Gao, Improving peroxymonosulfate activation by copper ion-saturated adsorbent-based single atom catalysts for the degradation of organic contaminants: electron-transfer mechanism and the key role of Cu single atoms, J. Mater. Chem. A 9 (2021) 11604–11613.

[106] X. Li, X. Huang, S. Xi, S. Miao, J. Ding, W. Cai, S. Liu, X. Yang, H. Yang, J. Gao, J. Wang, Y. Huang, T. Zhang, B. Liu, Single cobalt atoms anchored on porous N-doped graphene with dual reaction sites for efficient fenton-like catalysis, J. Am. Chem. Soc. 140 (2018) 12469–12475.

[107] Y. Yin, W. Li, C. Xu, L. Shi, L. Zhang, Z. Ao, M. Liu, M. Lu, X. Duan, S. Wang, S. Liu, H. Sun, Ultrafine copper nanoclusters and single sites for Fenton-like reactions with high atom utilities, Environ. Sci.: Nano 7 (2020) 2595–2606.

[108] Y. Liu, L. Qiu, Q. Nan, J. Wang, J.R. Zhao, T. Li, C. Hu, L. Hu, J. Tang, X. Liu, One-pot synthesis of mesoporous silicas supported Cu single-atom and CuO

nanoparticles for peroxymonosulfate-activated degradation of tetracycline over a wide pH range, Micro Mesopor. Mat. 333 (2022) 111729.

[109] X. Mao, Z. Deng, Y. Liu, H. Xie, Q. He, Y. Zhang, Z. Huang, H. Hu, T. Gan, Iron single atoms and clusters anchored on natural N-doped nanocarbon with dual reaction sites as superior Fenton-like catalysts, Appl. Surf. Sci. 597 (2022) 153625.

[110] B. Li, X. Cheng, R. Zou, X. Yong, C. Pang, Y. Su, Y. Zhang, Simple modulation of Fe-based single atoms/clusters catalyst with acidic microenvironment for ultrafast Fenton-like reaction, Appl. Catal. B 304 (2022) 121009.

[111] J. Li, Y. Zou, Z. Li, S. Fu, Y. Lu, S. Li, X. Zhu, T. Zhang, Modulating the electronic coordination configuration and d-band center in homo-diatomic Fe$_2$N$_6$ catalysts for enhanced peroxymonosulfate activation, ACS Appl. Mater. Interfaces 14 (2022) 37865–37877.

[112] B. Wang, C. Cheng, M. Jin, J. He, H. Zhang, W. Ren, J. Li, D. Wang, Y. Li, A Site distance effect induced by reactant molecule matchup in single-atom catalysts for fenton-like reactions, Angew. Chem. Int. Ed. 61 (2022) e202207268.

[113] G. Bi, R. Ding, J. Song, M. Luo, H. Zhang, M. Liu, D. Huang, Y. Mu, Discriminating the active Ru species towards the selective generation of singlet oxygen from peroxymonosulfate: nanoparticles surpass single-atom catalysts, Angew. Chem. Int. Ed. (2024) e202401551.

[114] C. Ling, X. Liu, H. Li, X. Wang, H. Gu, K. Wei, M. Li, Y. Shi, H. Ben, G. Zhan, C. Liang, W. Shen, Y. Li, J. Zhao, L. Zhang, Atomic-Layered Cu$_5$ nanoclusters on FeS$_2$ with dual catalytic sites for efficient and selective H$_2$O$_2$ activation, Angew. Chem. Int. Ed. 61 (2022) e202200670.

[115] C. Cheng, W. Ren, F. Miao, X. Chen, X. Chen, H. Zhang, Generation of Fe(IV)=O and its Contribution to Fenton-Like Reactions on a Single-Atom Iron-N-C Catalyst, Angew. Chem. Int. Ed. 62 (2023) e202218510.

[116] J. Song, N. Hou, X. Liu, M. Antonietti, Y. Wang, Y. Mu, Unsaturated single-atom CoN$_3$ sites for improved fenton-like reaction towards high-valent metal species, Appl. Catal. B 325 (2023) 122368.

[117] T. Ren, M. Yin, S. Chen, C. Ouyang, X. Huang, X. Zhang, Single-Atom Fe-N$_4$ sites for catalytic ozonation to selectively induce a nonradical pathway toward wastewater purification, Environ. Sci. Technol. 57 (2023) 3623–3633.

[118] K. Yin, R. Wu, Y. Shang, D. Chen, Z. Wu, X. Wang, B. Gao, X. Xu, Microenvironment modulation of cobalt single-atom catalysts for boosting both radical oxidation and electron-transfer process in Fenton-like system, Appl. Catal. B 329 (2023) 122558.

[119] J. Miao, J. Song, J. Lang, Y. Zhu, J. Dai, Y. Wei, M. Long, Z. Shao, B. Zhou, P.J. J. Alvarez, L. Zhang, Single-Atom MnN5 Catalytic Sites Enable Efficient Peroxymonosulfate Activation by Forming Highly Reactive Mn(IV)-Oxo Species, Environ. Sci. Technol. 57 (2023) 4266–4275.

[120] J. Wang, B. Li, Y. Li, X. Fan, F. Zhang, G. Zhang, W. Peng, Facile Synthesis of Atomic Fe-N-C Materials and Dual Roles Investigation of Fe-N$_4$ Sites in Fenton-Like Reactions, Adv. Sci. 8 (2021) 2101824.

[121] S. Shao, J. Cui, K. Wang, Z. Yang, L. Li, S. Zeng, J. Cui, C. Hu, Y. Zhao, Efficient and durable single-atom Fe catalyst for fenton-like reaction via mediated electron-transfer mechanism, ACS EST Engg 3 (2022) 36–44.

[122] J. Cui, S. Shao, J. Gao, Z. Yang, L. Li, S. Zeng, K. Wang, J. Cui, Y. Zhao, C. Hu, Efficient Single-Atom Fe-Catalyzed Fenton-like Reaction Involving Peroxymonosulfate for BPA Degradation by High-Valent Fe(IV)=O, ACS EST Water 2 (2022) 2698–2705.

[123] P. Yang, Y. Long, W. Huang, D. Liu, Single-atom copper embedded in two-dimensional MXene toward peroxymonosulfate activation to generate singlet oxygen with nearly 100% selectivity for enhanced Fenton-like reactions, Appl. Catal. B 324 (2023) 122245.

[124] X. Li, J. Hu, Y. Deng, T. Li, Z.-Q. Liu, Z. Wang, High stable photo-Fenton-like catalyst of FeP/Fe single atom-graphene oxide for long-term antibiotic tetracycline removal, Appl. Catal. B 324 (2023) 122243.

[125] C. Yang, S. Shang, Y. Fan, K. Shih, X.-Y. Li, L. Lin, Incorporation of atomically dispersed cobalt into the 2D metal–organic framework of a lamellar membrane for highly efficient peroxymonosulfate activation, Appl. Catal. B 325 (2023) 122344.

[126] R. Xie, K. Guo, Z. Ao, Z. Suo, H. Huang, D.Y.C. Leung, Surface-bound radicals generated from cobalt single-atom catalyst: Mechanism of boosting Fenton-like reactions, Chem. Eng. J. 461 (2023) 141920.

[127] M. Li, J. Chen, W. Wu, S. Wu, L. Xu, S. Dong, Diatomic Fe−Fe catalyst enhances the ability to degrade organic contaminants by nonradical peroxymonosulfate activation system, Nano Res 16 (2023) 4678–4684.

[128] Z. Zhao, W. Zhou, D. Lin, L. Zhu, B. Xing, Z. Liu, Construction of dual active sites on diatomic metal (FeCo−N/C-x) catalysts for enhanced Fenton-like catalysis, Appl. Catal. B 309 (2022) 121256.

[129] M. Abdul Nasir Khan, P. Kwame Klu, C. Wang, W. Zhang, R. Luo, M. Zhang, J. Qi, X. Sun, L. Wang, J. Li, Metal-organic framework-derived hollow Co$_3$O$_4$/carbon as efficient catalyst for peroxymonosulfate activation, Chem. Eng. J. 363 (2019) 234–246.

[130] Y. Wang, H. Sun, X. Duan, H.M. Ang, M.O. Tadé, S. Wang, A new magnetic nano zero-valent iron encapsulated in carbon spheres for oxidative degradation of phenol, Appl. Catal. B 172-173 (2015) 73–81.

[131] K. Li, S. Ma, S. Xu, H. Fu, Z. Li, Y. Li, S. Liu, J. Du, The mechanism changes during bisphenol A degradation in three iron functionalized biochar/peroxymonosulfate systems: the crucial roles of iron contents and graphitized carbon layers, J. Hazard. Mater. 404 (2021) 124145.

[132] H. Fu, P. Zhao, S. Xu, G. Cheng, Z. Li, Y. Li, K. Li, S. Ma, Fabrication of Fe$_3$O$_4$ and graphitized porous biochar composites for activating peroxymonosulfate to degrade p-hydroxybenzoic acid: Insights on the mechanism, Chem. Eng. J. 375 (2019) 121980.

[133] W. Ma, N. Wang, Y. Du, T. Tong, L. Zhang, K.-Y. Andrew Lin, X. Han, One-step synthesis of novel Fe$_3$C@nitrogen-doped carbon nanotubes/graphene nanosheets for catalytic degradation of Bisphenol A in the presence of peroxymonosulfate, Chem. Eng. J. 356 (2019) 1022–1031.

[134] B. Liu, W. Song, H. Wu, Y. Xu, Y. Sun, Y. Yu, H. Zheng, S. Wan, Enhanced oxidative degradation of norfloxacin using peroxymonosulfate activated by oily sludge carbon-based nanoparticles CoFe$_2$O$_4$/OSC, Chem. Eng. J. 400 (2020) 125947.

[135] X. Mi, P. Wang, S. Xu, L. Su, H. Zhong, H. Wang, Y. Li, S. Zhan, Almost 100% peroxymonosulfate conversion to singlet oxygen on single-atom CoN$_{2+2}$ sites, Angew. Chem. Int. Ed. 60 (2021) 4588–4593.

[136] B. Sheng, C. Deng, Y. Li, S. Xie, Z. Wang, H. Sheng, J. Zhao, In situ hydroxylation of a single-atom iron catalyst for preferential ^{1}O$_2$ production from H$_2$O$_2$, ACS Catal. 12 (2022) 14679–14688.

[137] L. Zhang, X. Jiang, Z. Zhong, L. Tian, Q. Sun, Y. Cui, X. Lu, J. Zou, S. Luo, Carbon Nitride Supported High-Loading Fe Single-Atom Catalyst for Activation of Peroxymonosulfate to Generate ^{1}O$_2$ with 100% Selectivity, Angew. Chem. Int. Ed. 60 (2021) 21751–21755.

[138] X. Ge, D. Xie, R.-f Cheng, W. Chen, C. Chen, F. Zhou, X. Wang, J.-j Chen, G.-p Sheng, Y. Wu, Three-dimensional welded Mn1 site catalysts with nearly 100% singlet oxygen fabrication for contaminant elimination, Precis. Chem. 1 (2023) 153–160.

[139] X. Zhao, X. Li, Z. Zhu, W. Hu, H. Zhang, J. Xu, X. Hu, Y. Zhou, M. Xu, H. Zhang, G. Hu, Single-atom Co embedded in BCN matrix to achieve 100% conversion of peroxymonosulfate into singlet oxygen, Appl. Catal. B 300 (2022) 120759.

[140] X. Liu, X. Yan, W. Liu, Q. Yan, M. Xing, Switching of radical and nonradical pathways through the surface defects of Fe$_3$O$_4$/MoO S in a Fenton-like reaction, Sci. Bull. (2023).

[141] J. Peng, P. Zhou, H. Zhou, W. Liu, H. Zhang, C. Zhou, L. Lai, Z. Ao, S. Su, B. Lai, Insights into the electron-transfer mechanism of permanganate activation by graphite for enhanced oxidation of sulfamethoxazole, Environ. Sci. Technol. 55 (2021) 9189–9198.

[142] A. Wang, P. Zhou, D. Tian, H. Zhang, Z. Xiong, Y. Du, C. He, Y. Yuan, T. Chen, Y. Liu, B. Lai, Enhanced oxidation of fluoroquinolones by visible light-induced peroxydisulfate: The significance of excited triplet state species, Appl. Catal. B 316 (2022) 121631.

[143] K. Qian, H. Chen, W. Li, Z. Ao, Y.-N. Wu, X. Guan, Single-Atom Fe catalyst outperforms its homogeneous counterpart for activating peroxymonosulfate to achieve effective degradation of organic contaminants, Environ. Sci. Technol. 55 (2021) 7034–7043.

[144] N. Jiang, H. Xu, L. Wang, J. Jiang, T. Zhang, Nonradical oxidation of pollutants with single-atom-Fe(III)-activated persulfate: Fe(V) being the possible intermediate oxidant, Environ. Sci. Technol. 54 (2020) 14057–14065.

[145] Y. Bao, C. Lian, K. Huang, H. Yu, W. Liu, J. Zhang, M. Xing, Generating High-valent Iron-oxo identical with Fe^{IV}=O Complexes in Neutral Microenvironments through Peroxymonosulfate Activation by Zn-Fe Layered Double Hydroxides, Angew. Chem. Int. Ed. 61 (2022) e202209542.

[146] F. Chen, L.L. Liu, J.H. Wu, X.H. Rui, J.J. Chen, Y. Yu, Single-Atom Iron Anchored Tubular g-C$_3$N$_4$ Catalysts for Ultrafast Fenton-Like Reaction: Roles of High-Valency Iron-Oxo Species and Organic Radicals, Adv. Mater. 34 (2022) 2202891.

[147] M. Yang, Z. Hou, X. Zhang, B. Gao, Y. Li, Y. Shang, Q. Yue, X. Duan, X. Xu, Unveiling the Origins of Selective Oxidation in Single-Atom Catalysis via Co-N$_4$-C Intensified Radical and Nonradical Pathways, Environ. Sci. Technol. 56 (2022) 11635–11645.

[148] S. Lan, B. Jing, C. Yu, D. Yan, Z. Li, Z. Ao, M. Zhu, Protrudent iron single-atom accelerated interfacial piezoelectric polarization for self-powered water motion triggered fenton-like reaction, Small 18 (2022) 2105279.

[149] S. Zuo, Z. Guan, F. Yang, D. Xia, D. Li, Reactive oxygen species regulation and synergistic effect for effective water purification through Fenton-like catalysis on single-atom Cu–N sites, J. Mater. Chem. A 10 (2022) 10503–10513.

[150] C. Zhang, L. Bai, M. Chen, X. Sun, M. Zhu, Q. Wu, X. Gao, Q. Zhang, X. Zheng, Z. Q. Yu, Y. Wu, Modulating the site density of Mo single atoms to catch adventitious O atoms for efficient H$_2$O$_2$ oxidation with light, Adv. Mater. 35 (2023) e2208704.

[151] X. Song, Y. Shi, Z. Wu, B. Huang, X. Wang, H. Zhang, P. Zhou, W. Liu, Z. Pan, Z. Xiong, B. Lai, Unraveling the discriminative mechanisms for peroxy activation via atomically dispersed Fe-N$_5$ sites for tunable water decontamination, Appl. Catal. B 340 (2024) 123240.

[152] J. Xu, X. Zheng, Z. Feng, Z. Lu, Z. Zhang, W. Huang, Y. Li, D. Vuckovic, Y. Li, S. Dai, G. Chen, K. Wang, H. Wang, J.K. Chen, W. Mitch, Y. Cui, Organic wastewater treatment by a single-atom catalyst and electrolytically produced H$_2$O$_2$, Nat. Sustain. 4 (2021) 233–241.

[153] Z. Wang, E. Almatrafi, H. Wang, H. Qin, W. Wang, L. Du, S. Chen, G. Zeng, P. Xu, Cobalt single atoms anchored on oxygen-doped tubular carbon nitride for efficient peroxymonosulfate activation: simultaneous coordination structure and morphology modulation, Angew. Chem. Int. Ed. 61 (2022) e202202338.

[154] B. Huang, X. Ren, J. Zhao, Z. Wu, X. Wang, X. Song, X. Li, B. Liu, Z. Xiong, B. Lai, Modulating electronic structure engineering of atomically dispersed cobalt catalyst in fenton-like reaction for efficient degradation of organic pollutants, Environ. Sci. Technol. 57 (2023) 14071–14081.

[155] B. Huang, Z. Wu, X. Wang, X. Song, H. Zhou, H. Zhang, P. Zhou, W. Liu, Z. Xiong, B. Lai, Coupled surface-confinement effect and pore engineering in a single-Fe-atom catalyst for ultrafast fenton-like reaction with high-valent iron-oxo complex oxidation, Environ. Sci. Technol. 57 (2023) 15667–15679.

[156] Q.Y. Wu, Z.W. Yang, Z.W. Wang, W.L. Wang, Oxygen doping of cobalt-single-atom coordination enhances peroxymonosulfate activation and high-valent

cobalt-oxo species formation, Proc. Natl. Acad. Sci. U. S. A. 120 (2023) e2219923120.

[157] X. Liang, D. Wang, Z. Zhao, T. Li, Y. Gao, C. Hu, Coordination number dependent catalytic activity of single-atom cobalt catalysts for fenton-like reaction, Adv. Funct. Mater. 32 (2022) 2203001.

[158] C. Chu, J. Yang, X. Zhou, D. Huang, H. Qi, S. Weon, J. Li, M. Elimelech, A. Wang, J.-H. Kim, Cobalt single atoms on tetrapyridomacrocyclic support for efficient peroxymonosulfate activation, Environ. Sci. Technol. 55 (2021) 1242–1250.

[159] Y. Zhang, X. Chen, C. Liang, L. Yin, Y. Yang, Reconstructing the coordination environment of single atomic Fe-catalysts for boosting the Fenton-like degradation activities, Appl. Catal. B 315 (2022) 121536.

[160] W. Ma, M. Sun, D. Huang, C. Chu, T. Hedtke, X. Wang, Y. Zhao, J.H. Kim, M. Elimelech, Catalytic membrane with copper single-atom catalysts for effective hydrogen peroxide activation and pollutant destruction, Environ. Sci. Technol. (2022) 8733–8745.

[161] J. Guo, Y. Wang, Y. Shang, K. Yin, Q. Li, B. Gao, Y. Li, X. Duan, X. Xu, Fenton- like activity and pathway modulation via single- atom sites and pollutants comediates the electron transfer process, Proc. Natl. Acad. Sci. U. S. A. 121 (2024) e2313387121.

[162] X. Wang, A. Vasileff, Y. Jiao, Y. Zheng, S.Z. Qiao, Electronic and structural engineering of carbon-based metal-free electrocatalysts for water splitting, Adv. Mater. 31 (2019) e1803625.

[163] H. Fu, J. Wei, G. Chen, M. Xu, J. Liu, J. Zhang, K. Li, Q. Xu, Y. Zou, W.-X. Zhang, S. Xi, X. Chen, S. Li, L. Ling, Axial coordination tuning Fe single-atom catalysts for boosting H_2O_2 activation, Appl. Catal. B 321 (2023) 122012.

[164] Y. Dou, C.T. He, L. Zhang, H. Yin, M. Al-Mamun, J. Ma, H. Zhao, Approaching the activity limit of $CoSe_2$ for oxygen evolution via Fe doping and Co vacancy, Nat. Commun. 11 (2020) 1664.

[165] M. Qian, X.L. Wu, M. Lu, L. Huang, W. Li, H. Lin, J. Chen, S. Wang, X. Duan, Modulation of Charge Trapping by Island-like Single-Atom Cobalt Catalyst for Enhanced Photo-Fenton-Like reaction, Adv. Funct. Mater. 33 (2023) 2208688.

[166] M. Liu, X. Wang, S. Cao, X. Lu, W. Li, N. Li, X.H. Bu, Ferredoxin-Inspired Design of S-Synergized Fe–Fe Dual-Metal Center Catalysts for Enhanced Electrocatalytic Oxygen Reduction Reaction, Adv. Mater. (2024) 2309231.

[167] B. Sun, H. Lv, Q. Xu, P. Tong, P. Qiao, H. Tian, H. Xia, Island-in-Sea Structured Pt3Fe Nanoparticles-in-Fe Single Atoms Loaded in Carbon Materials as Superior Electrocatalysts toward Alkaline HER and Acidic ORR, Small (2024) 2400240.

[168] Q. Wang, X. Huang, Z.L. Zhao, M. Wang, B. Xiang, J. Li, Z. Feng, H. Xu, M. Gu, Ultrahigh-Loading of Ir Single Atoms on NiO Matrix to Dramatically Enhance Oxygen Evolution Reaction, J. Am. Chem. Soc. 142 (2020) 7425–7433.

[169] H. Cheng, X. Wu, M. Feng, X. Li, G. Lei, Z. Fan, D. Pan, F. Cui, G. He, Atomically Dispersed Ni/Cu Dual Sites for Boosting the CO_2 Reduction Reaction, ACS Catal. 11 (2021) 12673–12681.

[170] H. Gu, X. Liu, X. Liu, C. Ling, K. Wei, G. Zhan, Y. Guo, L. Zhang, Adjacent single-atom irons boosting molecular oxygen activation on MnO_2, Nat. Commun. 12 (2021) 5422.

[171] X. Meng, C. Ma, L. Jiang, R. Si, X. Meng, Y. Tu, L. Yu, X. Bao, D. Deng, Distance Synergy of MoS_2-confined rhodium atoms for highly efficient hydrogen, Evol., Angew. Chem. Int. Ed. 59 (2020) 10502–10507.

[172] Z. Zhou, M. Li, Y. Zhang, L. Kong, V.F. Smith, M. Zhang, A.J. Gulbrandson, G. H. Waller, F. Lin, X. Liu, D.P. Durkin, H. Chen, D. Shuai, Fe-Fe Double-Atom Catalysts for Murine Coronavirus Disinfection: Nonradical Activation of Peroxides and Mechanisms of Virus Inactivation, Environ. Sci. Technol. 57 (2023) 3804–3816.

[173] L. Wang, H. Wang, J. Lu, Local chemical environment effect in single-atom catalysis, Chem. Catal. 3 (2023) 100492.

[174] Z.Y. Guo, C.X. Li, M. Gao, X. Han, Y.J. Zhang, W.J. Zhang, W.W. Li, Mn-O Covalency Governs the Intrinsic Activity of Co-Mn Spinel Oxides for Boosted Peroxymonosulfate Activation, Angew. Chem. Int. Ed. 60 (2021) 274–280.

[175] Z. Chen, X. Zhang, W. Liu, M. Jiao, K. Mou, X. Zhang, L. Liu, Amination strategy to boost the CO_2 electroreduction current density of M-N/C single-atom catalysts to the industrial application level, Energy Environ. Sci. 14 (2021) 2349–2356.

[176] Y. Zou, J. Hu, B. Li, L. Lin, Y. Li, F. Liu, X.-Y. Li, Tailoring the coordination environment of cobalt in a single-atom catalyst through phosphorus doping for enhanced activation of peroxymonosulfate and thus efficient degradation of sulfadiazine, Appl. Catal. B 312 (2022) 121408.

[177] X. Zhou, M.K. Ke, G.X. Huang, C. Chen, W. Chen, K. Liang, Y. Qu, J. Yang, Y. Wang, F. Li, H.Q. Yu, Y. Wu, Identification of Fenton-like active Cu sites by heteroatom modulation of electronic density, Proc. Natl. Acad. Sci. U. S. A. 119 (2022) e2119492119.

[178] H. Yu, J. Ji, Q. Yan, M. Xing, Transition metal phosphides for heterogeneous Fenton-like oxidation of contaminants in water, Chem. Eng. J. 449 (2022) 137856.

[179] J. Miao, Y. Zhu, J. Lang, J. Zhang, S. Cheng, B. Zhou, L. Zhang, P.J.J. Alvarez, M. Long, Spin-State-dependent peroxymonosulfate activation of single-atom M–N moieties via a radical-free pathway, ACS Catal. 11 (2021) 9569–9577.

[180] F. Liu, Y. Ren, J. Duan, P. Deng, J. Lu, H. Ge, X. Liu, Q. Xia, H. Qi, N. Yang, Y. Qin, Axial nitrogen-coordination engineering over Fe-N_x active species for enhancing Fenton-like reaction performance, Chem. Eng. J. 454 (2023) 140382.

[181] J. Yang, D. Zeng, J. Li, L. Dong, W.-J. Ong, Y. He, A highly efficient Fenton-like catalyst based on isolated diatomic Fe-Co anchored on N-doped porous carbon, Chem. Eng. J. 404 (2021) 126376.

[182] Q. Wang, C. Liu, D. Zhou, X. Chen, M. Zhang, K. Lin, Degradation of bisphenol a using peroxymonosulfate activated by single-atomic cobalt catalysts: different reactive species at acidic and alkaline pH, Chem. Eng. J. 439 (2022) 135002.

[183] H. Dai, W. Zhou, W. Wang, Z. Liu, Unveiling the role of cobalt species in the Co/ N-C catalysts-induced peroxymonosulfate activation process, J. Hazard. Mater. 426 (2022) 127784.

[184] J. Shan, C. Ye, Y. Jiang, M. Jaroniec, Y. Zheng, S.-Z. Qiao, Metal-metal interactions in correlated single-atom catalysts, Sci. Adv. 8 (2022) eabo0762.

[185] Y. Guo, M. Wang, Q. Zhu, D. Xiao, D. Ma, Ensemble effect for single-atom, small cluster and nanoparticle catalysts, Nat. Catal. 5 (2022) 766–776.